

**Estimation of source fault parameters  
from tsunami deposits  
by inverse model using deep neural network**

Yasutaka Iijima

*Doctoral Thesis*

*Department of Geology and Mineralogy  
Division of Earth and Planetary Sciences  
Graduate School of Science  
Kyoto University*

*February, 2024*

## **Abstract**

Tsunami deposits are valuable clues to estimate the magnitudes of past tsunami events, which are essential for risk assessment towards disaster prevention. Here, a new inverse model is proposed to estimate the wave-source fault parameters of the tsunami from tsunami deposits. The model using the deep neural network (DNN) was trained with artificial datasets produced by the forward model calculation of tsunamis. Firstly, the model was trained to estimate the parameters of the fault model with homogeneous slip from tsunami deposits. The model was validated with synthetic datasets, reconstructing the fault parameters accurately from the properties of tsunami deposits. Then, an inverse analysis was performed to the 2011 Tohoku-oki tsunami deposit on Sendai Plain to test the model's applicability to natural cases. The 2011 Tohoku-oki tsunami is the ideal event to validate the method for estimating past tsunami magnitudes because the source fault, behavior, and deposits of the tsunami have been investigated quantitatively in detail. As a result, the inverse model predicted 21.3 m in fault slip, 119.9 km in fault width, and 8.9 in the moment magnitude. These values were consistent with the estimation by the existing geodetic and seismological studies. Secondly, the model was improved to estimate the fault model parameters with the heterogeneous slip. The width, length, and location of the source fault were estimated from the characteristics of the tsunami deposits across diverse regions. The model was again validated with synthetic datasets, and then an inverse analysis of the 2011 Tohoku-oki tsunami was performed on the deposits observed in three regions: Rikuzentakata, Sendai, and Odaka. The model predicted 464.5 km in fault length and 162.0 km in fault width, and the northeast edge of the fault to be

196.9 km from the edge of the Japan Trench. The moment magnitude of the source fault was calculated as 9.0, again consistent with the value 9.0–9.1 obtained from the geodetic or seismological methods. This study developed the inverse model to estimate source fault parameters solely from tsunami deposits. Therefore, unlike other methods, it can also evaluate information about the earthquake faults that have generated historic or prehistoric tsunamis to contribute to assessing the risk of regional tsunami hazards from the geologic records of past tsunamis in various regions.

# Table of Contents

Abstract .....	i
Table of Contents.....	iii
<b>Chapter 1. Introduction .....</b>	<b>1</b>
<b>1.1 Characteristic features of tsunami deposits.....</b>	<b>1</b>
<b>1.2 Historical review of tsunami deposit research .....</b>	<b>3</b>
<b>1.3 Past attempts for quantitative estimation of past tsunami characteristics from paleo-tsunami deposits .....</b>	<b>7</b>
<b>1.4 Inverse analysis of tsunami deposits.....</b>	<b>9</b>
<b>1.5 Significance to estimate fault parameters from tsunami deposits .....</b>	<b>11</b>
<b>1.6 Challenges in tsunami deposit research.....</b>	<b>13</b>
<b>1.7 Research objective .....</b>	<b>15</b>
<b>Chapter 2. Methodology.....</b>	<b>17</b>
<b>2.1 Introduction.....</b>	<b>17</b>
<b>2.2 Forward model of tsunami propagation and sediment transportation.....</b>	<b>17</b>
<b>2.3 Inverse model for tsunami deposit using DNN .....</b>	<b>21</b>
<b>2.4 Summary.....</b>	<b>23</b>
<b>Chapter 3. Reconstruction of fault parameters from tsunami deposits.....</b>	<b>24</b>
<b>3.1 Introduction.....</b>	<b>24</b>
<b>3.2 Method .....</b>	<b>26</b>
<b>3.2.1 Forward model for tsunami propagation and sediment transportation.....</b>	<b>26</b>
<b>3.2.2 Inverse model using deep neural network.....</b>	<b>30</b>
<b>3.2.3 Jackknife error estimation.....</b>	<b>32</b>
<b>3.3 Result .....</b>	<b>33</b>
<b>3.3.1 Training of inverse model and validation with synthetic data .....</b>	<b>33</b>
<b>3.3.2 Inverse analysis of the 2011 Tohoku-oki tsunami and error estimation .....</b>	<b>36</b>
<b>3.3.3 Estimated behavior of the tsunami inundation flow and depositional features..</b>	<b>39</b>
<b>3.4 Discussion .....</b>	<b>43</b>
<b>3.4.1 Reconstructed fault parameters of the 2011 Tohoku-oki tsunami deposit.....</b>	<b>43</b>
<b>3.4.2 Advantage of proposed 2D inverse model for tsunami deposits and future challenges.....</b>	<b>43</b>
<b>3.5 Conclusions.....</b>	<b>44</b>
<b>Chapter 4. Estimation of parameters of source fault model with heterogenous slip from tsunami deposits across diverse regions by DNN inverse model .....</b>	<b>46</b>

<b>4.1</b>	<b>Introduction</b> .....	46
<b>4.2</b>	<b>Method</b> .....	47
<b>4.2.1</b>	<b>Source fault model</b> .....	47
<b>4.2.2</b>	<b>Topographic settings and depositional features of the study areas</b> .....	50
<b>4.2.3</b>	<b>Forward model calculation for producing training and test datasets</b> .....	57
<b>4.2.4</b>	<b>Training of inverse model using deep neural network</b> .....	59
<b>4.3</b>	<b>Result</b> .....	61
<b>4.3.1</b>	<b>Training of inverse model and validation with synthetic data</b> .....	61
<b>4.3.2</b>	<b>Inverse analysis of the 2011 Tohoku-oki tsunami</b> .....	68
<b>4.4</b>	<b>Discussion</b> .....	73
<b>4.4.1</b>	<b>Comparison with fault parameters determined by existing studies</b> .....	73
<b>4.4.2</b>	<b>Advantage and limitation of the model</b> .....	74
<b>4.5</b>	<b>Conclusions</b> .....	75
<b>Chapter 5.</b>	<b>Conclusions</b> .....	77
<b>5.1</b>	<b>Chapter summaries</b> .....	77
<b>5.2</b>	<b>Future research directions</b> .....	78
<b>Notation</b>	.....	80
<b>Acknowledgement</b>	.....	82
<b>Reference</b>	.....	83

## **Chapter 1. Introduction**

A tsunami is a wave with an extraordinarily long wavelength (Robke and Vott, 2017). It is caused by a variety of geological processes, such as earthquakes (Mori et al., 2012), landslides (Bondevik et al., 2012), volcanic eruptions (Omira et al., 2022), and bolide impacts (Matsui et al., 2002). Tsunamis are severe natural hazards that affect the safety and sustainability of human society. In the case of the 2011 off the Pacific coast of the Tohoku earthquake and tsunami, total deaths reached 19,729 people, and 2,559 persons are still missing (Fire and Disaster Management Agency, 2020).

Tsunami deposits are the only direct trace of past tsunamis. Once a tsunami occurs, it leaves a geological trace of a tsunami in the environment, from deep seafloors (Cita et al., 1996) to coastal onshore areas (Goto et al., 2011). The investigation of the frequency and size of past tsunamis to assess the regional risks of the disaster caused by tsunamis and tsunami deposits are known to be essential sources of information to evaluate past events in a particular region, providing quantitative evidence of both the age and the magnitude of past tsunamis (Goto et al., 2021).

This study aims to establish a method to reconstruct the magnitude of past tsunamis from tsunami deposits quantitatively. In the following section of this chapter, the past studies of tsunami deposits are reviewed, and the issues of the previous studies are summarized. Then, the specific target of this study is presented.

### **1.1 Characteristic features of tsunami deposits**

Tsunami deposits, or “tsunamiites” (Shiki and Yamazaki, 2008), are sediments eroded, transported, and deposited by tsunamis. Tsunami deposits can be composed of any size of sedimentary grains available in the source area, but sandy tsunami deposits observed

in coastal areas were widely recognized as the most common type of geological traces of tsunami since the initial study age of this research field (e.g., Atwater, 1987, Minoura and Nakaya, 1991). General characteristics of sandy tsunami deposits, which have been reviewed in several articles (e.g., Goff et al., 2012), are fining inland and upward trend (Fujino et al., 2010), thinly bedded ranging from several centimeters to several dozen centimeters (Abe et al., 2012), and large extension for several kilometers inland and tens or hundreds of kilometers alongshore depending on the magnitudes of the tsunamis.

Each tsunami wave can form a distinct sedimentary unit, and the lower contact of each unit is usually unconformable or erosional (Naruse et al., 2012). Sedimentary structures, such as normal grading (Paris et al., 2007) or inverse grading (Naruse et al., 2010, 2012; Iijima et al., 2021), are commonly observed, reflecting the behavior of tsunami inundation flows. The flow directions of tsunamis may reverse because of the transition between the flooding and the ebb currents, which can be detected by the cross-lamination or grain fabric analysis of tsunami deposits (Takashimizu et al., 2012).

Sandy tsunami deposits are formed in various terrestrial regions, including lakes and alluvial plains (Sawai et al., 2012). In particular, they have been surveyed in marshes between beach ridges because they are intercalated in peats or muddy deposits generally deposited in such areas. Sandy tsunami deposits can be easily detected in such heterolithic successions (Sawai et al., 2012). Similar to sandy tsunami deposits, tsunami boulders, sometimes exceeding 10 m in diameter, are prominent traces of past tsunamis. Calculating the velocity that can transport such massive particles helps estimate the minimum velocities of tsunami inundation flows (Goto et al., 2007).

Traces of tsunamis are also discovered on the deep seafloor. Several turbidites deposited from tsunami-induced turbidity currents have been reported in deep-sea

environments (Arai et al., 2013).

## **1.2 Historical review of tsunami deposit research**

Onshore modern tsunami deposits have been intensively studied, especially for the past 20 years (Costa and Andrade, 2020), in response to the occurrences of large tsunamis such as the 2004 Indian Ocean tsunami and the 2011 Tohoku-oki tsunami, while the initial study of the modern tsunami deposit was published more than 60 years ago. The Pacific coast of Northeastern Japan has repeatedly suffered from large tsunamis, so that research on tsunami deposits has begun in this region. Kon'no (1961) was the first study of the modern tsunami deposits, which described sedimentological characteristics of tsunami deposits caused by the 1960 Chilean tsunami based on the post-event survey by Tohoku University. The tsunami was caused by the trench-axis-type earthquake along the Chilean subduction zone, which propagated to the other side of the Earth. Subsequently, the Chilean tsunami caused severe damage in the coastal regions of Northeastern Japan. Kon'no (1961) reported characteristics of traces of the Chilean tsunami, such as erosional scours along the shoreline and sandy deposits left in the inland regions.

Early examples of studies on tsunami deposits were concentrated in the 1980s to 1990s. In 1983, the Sea of Japan tsunami occurred in the Sea of Japan offshore northeastern Japan, and sandy tsunami deposits were observed in the lacustrine succession of Lake Jusan, Aomori Prefecture, Japan (Minoura et al., 1987). The findings that modern tsunami deposits can be preserved in lacustrine environments led to exploring paleo-tsunami deposits in similar environments (Minoura et al., 1994). At the same time, the initial research on the paleo-tsunami deposit was conducted around the Cascadian Subduction Zone, North America, which implied the occurrence of the undescribed

prehistoric large earthquake (Atwater, 1987).

In some cases, studies of the modern tsunami deposits have led to attempts to explore past tsunami records. The 1993 Hokkaido Nansei-oki earthquake caused a large tsunami, which deposited the tsunami deposit in the western Okushiri Island, Hokkaido, Japan (Sato et al., 1995). In addition to this modern tsunami deposit, several layers of the paleo-tsunami deposits were discovered in the region, leading to a comparison of sedimentary features between the modern and paleo-tsunami deposits (Nishimura and Miyaji, 1995; Sato et al., 1995). Nishimura and Miyaji (1995) interpreted that the origin of the paleo-tsunami deposits was not necessarily earthquakes. Instead, they suggested that the volcanic eruptions were also candidates for the tsunami wave source. In this period, most studies on the tsunami deposits focused on the Holocene events, mainly because they are relatively thin (less than half a meter in most cases), making their preservation in the geological records difficult. Nonetheless, Bourgeois et al. (1988) discovered the end-Cretaceous tsunami deposit caused by the bolide impact, which caused the Cretaceous-Paleogene mass extinction event.

One of the best-studied paleo-tsunami deposits is the 869 Jogan tsunami deposit (Minoura and Nakaya, 1991; Minoura et al., 2001). The uniqueness of the 869 Jogan tsunami is that the tsunami was recorded in the historical document even though it occurred more than 1100 years ago. The Sandai-jitsuroku, an official Japanese history compiled in A.D. 901, described that Northeast Japan suffered from a large tsunami in A.D. 869, named the Jogan tsunami (Minoura and Nakaya, 1991). The field survey of the subsurface successions of the Sendai Plain,  $^{14}\text{C}$  age dating, and the paleontological study of the fossil diatoms inferred that the Jogan tsunami left the sandy tsunami deposit in the broad region of the area. In addition, the tephra bed, known as Towada-A Tephra, was

observed just above the tsunami deposit (Minoura et al., 2001), making it easy to correlate the tsunami deposit among the broad regions. In addition to sedimentological analysis, utilization of the historical documents, biological analysis, and the hydrodynamic simulation of the tsunami qualitatively reconstructed the past tsunami behavior that occurred more than 1100 years ago (Minoura et al., 2001). However, the source fault parameters of the tsunami were estimated only based on the description of the historical document about the building damage and the moment magnitudes of the modern earthquakes around the area. The tsunami deposit was not directly used to reconstruct the fault parameters.

Although a few groups intensively studied tsunami deposits at that time, the occurrence of the 2004 Indian Ocean tsunami led to more attention to tsunami deposits, resulting in the development of this research area. The 2004 Indian Ocean tsunami occurred on 26<sup>th</sup> December 2004, triggered by a moment magnitude (M<sub>w</sub>) 9.1 earthquake. The tsunami caused severe damage to coastal areas of southeast Asia, such as Indonesia and Thailand. Field surveys were conducted to investigate various sedimentological aspects of tsunami deposits, such as fining upward and landward trends (Fujino et al., 2010), inverse grading (Naruse et al., 2010), mineralogical assemblages (Costa et al., 2015; Pham et al., 2017), death assemblage of diatoms (Sawai et al., 2009). The sediment source and depositional process of tsunami deposits were discussed in detail from those multiple pieces of evidence. In addition to sandy tsunami deposits, tsunami boulders were evaluated quantitatively to reconstruct the tsunami inundation flow (Goto et al., 2007). Geomorphological change before and after the tsunami event was investigated to discuss the erosional process of the tsunami (Pari et al., 2008; Masaya et al., 2019).

In addition to these modern tsunami deposits in Southeast Asia, the paleo-

tsunami deposit was discovered on Phra Thong Island, Thailand, which suffered from the 2004 Indian Ocean tsunami (Jankaew et al., 2008; Fujino et al., 2009). A comparison between the modern and the paleo-tsunami deposits was conducted to discuss the recurrence interval and magnitudes of paleo-tsunami events (Fujino et al., 2009; Rubin et al., 2017; Philibosian et al., 2017). Since the area has also suffered from tropical storms, the difference between modern storm deposits and tsunami deposits was investigated to distinguish tsunami deposits from other event deposits (Morton et al., 2007; Phantuwongraj and Choowong, 2012).

The 2011 off the Pacific coast of Tohoku Earthquake Tsunami (hereafter, the 2011 Tohoku-oki tsunami), which caused severe damage along the Pacific coast of northeastern Japan (Fire and Disaster Management Agency, 2020), brought significant progress in the research of tsunami deposits. After the 2011 Tohoku-oki tsunami, a large number of studies have been conducted focusing on various aspects, dealing with the sedimentological (e.g., Goto et al., 2011; Abe et al., 2012; Jagodziński et al., 2012; Nakamura et al., 2012; Naruse et al., 2012; Takashimizu et al., 2012; Fujiwara and Tanigawa, 2014; Matsumoto et al., 2016; Abe et al., 2020), geochemical (e.g., Chagué-Goff et al., 2012), and paleontological characteristics of the tsunami deposits (e.g., Szczuciński et al., 2012) (see also a review by Goto et al., 2021). Although many studies have focused on sandy tsunami deposits, the significance of muddy tsunami deposits was also recognized because they were distributed near the inundation limits, making it possible to estimate the inundation limits of past tsunamis (Shinozaki et al., 2015). Further detailed properties of tsunami deposits, such as grain shapes of gravelly tsunami deposits, have been revealed to help identify the source of tsunami deposits (Ishimura and Yamada, 2019). Video recording during tsunami inundation provided the hydraulic conditions of

the tsunami inundation flow (Sanuki et al., 2013; Hayashi and Koshimura, 2013).

As described above, the investigation of modern tsunami deposits and the observational datasets of tsunami behaviors have revealed the sedimentary processes of tsunamis. The sedimentological studies of modern tsunami deposits have helped distinguish tsunami deposits from other event deposits, such as sand layers from storms or floodings. Description of the modern tsunami and storm deposits, such as their lateral continuity or vertical variation in grain size and sedimentary structures, highlighted their discriminative features, and thus, further case studies will essentially contribute to this research field (Morton et al., 2007).

### **1.3 Past attempts for quantitative estimation of past tsunami characteristics from paleo-tsunami deposits**

Tsunami deposits are preserved in geological records and have been utilized to estimate the magnitudes of past tsunamis. Significantly, the historical and geological records implied that the Pacific coast of northeastern Japan especially suffered from large-scale tsunamis repeatedly (Goto et al., 2021), which led to intensive studies on estimating magnitudes of past tsunamis and earthquakes in this area. Among these tsunamis, some were estimated to have originated from Japan Trench repeatedly as subduction zone earthquakes, such as the 869 Jogan tsunami (e.g., Minoura et al., 2001; Namegaya et al., 2010) or the Keicho tsunami that occurred in A.D. 1611 (Hatori, 2009). However, while the similarity in the extent and displacement of the source fault should be considered to discuss the recurrence cycle of earthquakes, such data are not available for past tsunamis.

The magnitude of the Jogan earthquake was estimated using the tsunami deposit (Satake et al., 2008; Sugawara et al., 2013). Satake et al. (2008) compared the distribution of the tsunami deposit and the inundation area of the tsunami estimated by the forward

model calculations at two regions, Sendai and Ishinomaki Plains, providing constraints for the wave source fault parameters. Their estimation, however, was based on only 10 case studies of numerical simulations, and thus, further optimal or equivalent solutions may be found if more cases are explored. Their study did not utilize detailed information on depositional features of tsunami deposits, such as thickness or grain-size distributions.

In Ishigaki island, southwest Japan, the magnitude of the historical tsunami was estimated using both historical documents and the distribution of tsunami boulders. Based on the distribution of tsunami boulders (Goto et al., 2010), the magnitude of the A.D. 1771 Meiwa tsunami was estimated (Miyazawa et al., 2012).

Tsunamis are generated not only by earthquakes but also by bolide impacts, and it is also targeted for evaluating magnitudes of tsunami and their source events. Wave heights of tsunamis caused by the end-Cretaceous bolide impact were estimated by calculating the forward model of tsunami propagation, assuming that the impact instantaneously evaporated all seawater in the crater region (Matsui et al., 2002). Estimating the magnitudes of tsunamis caused by bolide impacts may also provide a better understanding of the surface environments of other planets. For example, it is controversial whether there was an ocean on Mars in the past. If the ocean existed on the Martian surface, a bolide impact on the Martian ocean should have caused a tsunami, which is expected to leave traces such as transported boulders or scours (Iijima et al., 2014). Thus, the tsunami-transported boulders can be traces of tsunamis indicative of the past ocean. Iijima et al. (2014) conducted a numerical simulation of an impact-induced tsunami on Mars, assuming that the ocean's existence and the tsunami occurred by the bolide impact at the observed crater. They estimated the size of the boulder that was possibly transported by the impact-induced tsunami, which will help detect the magnitude

of Martian tsunamis in future studies.

The studies introduced above attempted to estimate the magnitudes of tsunami events quantitatively. However, they conducted limited numbers of numerical experiments and did not exhaustively explore the possible parametric space of hydraulic conditions of tsunamis or source fault properties. Whereas the research on tsunami boulders or the analysis of the critical flow velocity of sand particles provides estimates of the minimum flow velocities of the inundation flows, those models cannot provide information on the most probable flow conditions. Therefore, inverse analysis of tsunami deposits to exhaustively explore the parametric space is essential for quantitative reconstruction of hydraulic condition or wave source information of tsunami.

#### **1.4 Inverse analysis of tsunami deposits**

The inverse analyses of tsunami deposits (Fig. 1-1) have been developed to reconstruct the hydraulic conditions of tsunamis based on the depositional characteristics of tsunami deposits. For instance, Moore et al. (2007) estimated the shear velocity of the tsunami inundation flow from the grain size information of the tsunami deposit at a single location. Jaffe and Gelfenbuam (2007) developed the tsunami sediment transport model (TsuSedMod) that can estimate tsunami flow speed as a function of grain size and flow depth. Soulsby et al. (2007) reconstructed the maximum flow depth and inundation distance using a simple one-dimensional cross-sectional tsunami propagation model, assuming uniform velocity, no bottom sediment entrainment, and a constant flat slope topography. However, the verification by the modern tsunamis implied that the oversimplification of their forward modeling did not adequately reproduce the complex behavior of actual tsunamis (Fig. 1-2) and tended to overestimate or underestimate the scale of the flow (Sugawara et al., 2014).

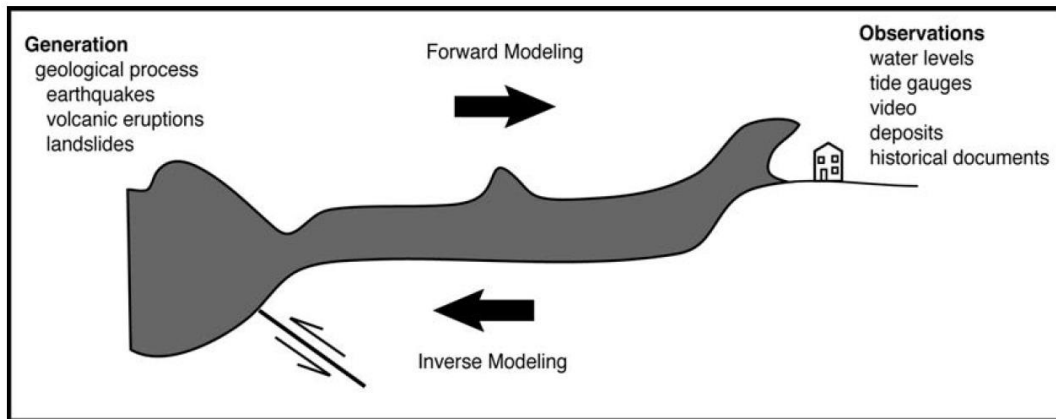


Fig. 1-1. Schematic image of forward and inverse model of tsunami (Jaffe et al., 2016)

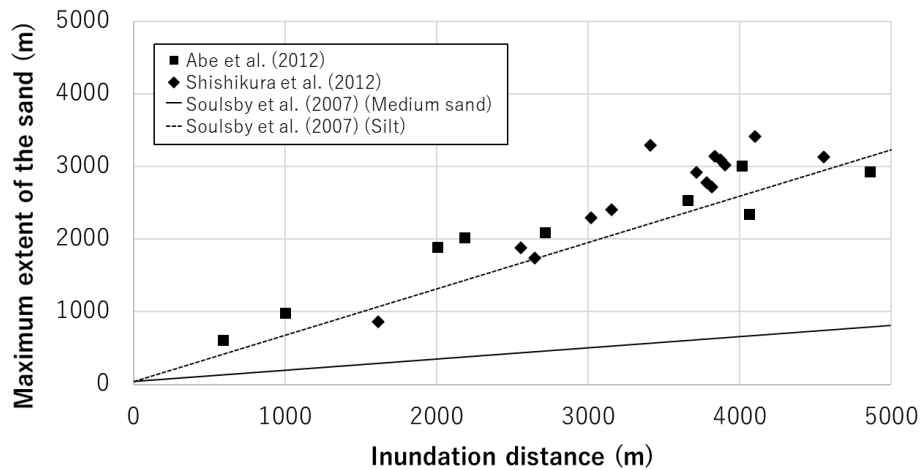


Fig. 1-2. Comparison between the result of the inverse model and actual sediment distribution of the 2011 Tohoku-oki tsunami deposit on Sendai Plain. Although medium sand is dominant in the study area, measured distribution matches the result of the inverse model, which assumes silt. (the data is plotted based on Sugawara et al. (2014)).

Recently, an inversion method for tsunami deposits was proposed, combining the 1D forward model and deep neural network (DNN) (Mitra et al., 2020, 2021). In their method, a 1D forward model FITNUSS (Naruse and Abe, 2017) was calculated repeatedly by changing initial parameters to produce datasets of thickness and grain size distributions of onshore tsunami deposits. Then, the combination of initial parameters and

depositional features of onshore tsunami deposits was used as a training dataset for the DNN inverse model to explore their relationship. The trained inverse model can estimate the initial hydraulic parameters of tsunamis from the information on onshore tsunami deposits. The model was applied to the actual tsunami deposits in the Sendai Plain, Japan, and Koh Phra Thong, Thailand, and it reconstructed reasonable values of the hydraulic conditions around the shoreline for the 2011 Tohoku-oki and 2004 Indian Ocean tsunamis, respectively (Mitra et al., 2020, 2021).

On the other hand, the simplified 1D models employed in the existing inverse models have several limitations. For example, the 1D forward model FITTNUSS assumes a flat topography so that it cannot consider the behavior of tsunamis on complex topography. Thus, it was difficult to perform the inverse analysis of tsunamis that run up topography, such as narrow valleys or developed areas with various artificial structures. In addition, the previous model can only reconstruct the initial hydraulic conditions of tsunamis, such as wave heights and velocities around the shoreline. These approaches cannot infer information on tsunami source faults even if inverse analyses of tsunami deposits are successful.

### **1.5 Significance to estimate fault parameters from tsunami deposits**

Accurate estimation of fault parameters of tsunami sources is essential for the risk assessment of tsunamis. The entire behavior of tsunamis can be predicted from the fault parameters of the wave source using the 2D forward model calculation (e.g., Satake et al., 2013). Thus, assessing the fault parameters of repeated large tsunamis contributes to disaster prevention planning for future events.

Therefore, a methodology is required for predicting the fault parameters of wave sources of past tsunamis. Although historical documents may provide information on past

tsunami occurrences, the properties of the tsunami wave sources are hardly reconstructed. Several studies have estimated the fault parameters of modern tsunamis, including the 2011 Tohoku-oki tsunami. However, the method has yet to be established for past tsunamis. For example, Imamura et al. (2012) estimated fault parameters of the 2011 Tohoku-oki tsunami based on the inundation area along the Pacific coast of northeastern Japan (Imamura et al., 2012). Satake et al. (2013) utilized the time series of wave heights observed at the points in the coastal and offshore regions to estimate fault extent and displacement. These methods successfully estimated the fault parameters, but it is evident that they are not applicable to past tsunamis because wave height or inundation areas are not measurable for past tsunamis.

In this term, tsunami deposits are essential sources of information to reconstruct the scale of past tsunamis. Few attempts were made to reconstruct fault parameters solely from tsunami deposits. Sugawara et al. (2011) attempted to estimate fault parameters from the tsunami deposits. They estimated the region and slip length of the source of the 869 Jogan tsunami from the distribution and grain size of the tsunami deposit. Comparing the simulation results of the tsunami inundation areas and the critical shear velocity of sediment transport with the measured depositional features onshore area, they determined reasonable sets of fault parameters for the Jogan tsunami. However, they tested only 12 cases and did not exhaustively search for the possible fault parameters. Furthermore, various informative depositional features, such as thickness and grain size distribution, were not utilized to estimate the inundation flow behavior. The computational costs of searching the optimal parameters of the complex tsunami forward model disturbed further inverse modeling of tsunami deposits in past studies.

## **1.6 Challenges in tsunami deposit research**

Previous studies reviewed above imply that there are still challenges in research of tsunami deposits, including (1) identification of paleo-tsunami deposits in geological records, (2) age determination of paleo-tsunami deposits, (3) evaluation of artificial structure influences to modern tsunami behavior, and (4) quantitative estimation of magnitudes of past tsunamis and source events from tsunami deposits.

(1) Identification of tsunami deposits is to recognize the characteristics and behavior of tsunamis peculiar to other depositional processes. Depositional characteristics of tsunami deposits, such as normal grading, multiple-layered bedding, and the landward fining trend, have been interpreted as the consequences of specific behaviors of tsunamis (Goff et al., 2012). For example, the multiple-layered feature of tsunami deposits has been attributed to the reversal of flow directions of tsunamis, which must not be observed in the case of storm surges (Naruse et al., 2010). Background lithologies are also significant for detecting thin-bedded sand layers of tsunami deposits. Sawai et al. (2012) describe appropriate topography for searching tsunami deposits. For instance, tsunami deposits intercalated in peats formed in a marsh environment can be readily identified because of lithological differences.

(2) Age determination of tsunami deposits is also significant but challenging.  $^{14}\text{C}$  dating of samples taken from the horizon just above and below the tsunami deposit in succession has been used chiefly for the Holocene tsunami deposit (Minoura et al., 2001). Tephra beds near tsunami deposits are also helpful for age determination if the bed can be correlated to the tephra in which the absolute ages are known. However, these methods cannot directly estimate the ages of tsunami events. Recently, high-resolution radiocarbon measurements for the entire geological section and statistical interpolation for

accumulation rates of background deposits enabled high-precision dating of tsunami deposits (Ishizawa et al., 2017, 2019). Historical records are also helpful in supporting the age interpretation of geological records.

(3) One difficulty in examining the sedimentary processes of tsunamis from modern tsunami deposits is to evaluate the effect of artificial structures. Most studies selected the survey area where the artificial structures were less common because their research objectives were to apply the understanding of modern events to the paleo-tsunami deposits that were generally formed without any artificial structures. However, it is difficult to avoid the influences of artificial structures in developed countries completely. In the case of the 2011 Tohoku-oki tsunami, the artificial structures inevitably affected the inundation flows of the tsunami. For instance, Sugawara and Goto (2012) revealed that the tsunami flow velocity on paddy fields on the Sendai Plain was significantly decelerated and then accelerated again by a roadway that is located 1.6 km landward from the shoreline and is transverse to the flow direction. Furthermore, the erosional features of the tsunami were developed around the artificial topographic highs along the shoreline of the Sendai Plain, including a coastal dike (Nemoto and Minoura, 2012), a hill (Richmond et al., 2012), and the lower side of ~50-cm high banks of the rice paddy fields (Fujiwara and Tanigawa, 2014). Iijima et al. (2021) evaluated the effects of artificial structures on the erosional and depositional process of tsunami deposits in the Odaka area of Minami-soma city, Fukushima prefecture, concluding that the location of the sediment source area was determined by the presence of the coastal dike just seaward of the source area. In addition, the roads on the paddy field banks influenced the thickness and sedimentary structures of the tsunami deposit. The 1D and 2D numerical models of tsunami propagation can reasonably predict the behavior of the tsunami on the topography

with the artificial structures (Sugawara and Goto, 2012; Iijima et al., 2021). Thus, modern tsunami deposit studies have implied the importance of incorporating local topographic effects into the forward model for estimating the behaviors of tsunamis and resultant tsunami deposits.

(4) Quantitative reconstruction of tsunamis and source events is urgent for disaster prevention. For example, planning for the disaster prevention of the Nankai trough earthquake requires consideration of the maximum case scenario (Central Disaster Prevention Council, 2011), while it remains unknown which of the five fault segments near the trench have moved in a couple in the past. Thus, predicting the realistic maximum case scenario from the geological records of past events is essential for developing appropriate disaster prevention.

This study focused on the fourth challenge of the tsunami deposit research. Tsunami deposits are valuable clues to estimate the magnitudes of past tsunami events. However, the previous inverse model can not estimate source fault information. This study proposed a new inverse model of tsunami deposits using a DNN that enables the estimation of source fault parameters solely from tsunami deposits.

## **1.7 Research objective**

The objectives of this study are (1) to develop a 2D inverse model using DNN to perform an inverse analysis of tsunami deposits on complex topography and (2) to estimate the source fault model solely from tsunami deposits. The developed models are verified with the measured datasets of the actual modern tsunami deposits.

Chapter 2 describes the forward and inverse models used in this study. The models in this study employed Delft3D-FLOW as the forward model, a 2D shallow-water model to calculate tsunami propagation, inundation, and sediment transportation to

incorporate actual topography. The DNN inverse model was trained with the artificial datasets produced by repetition of the forward model calculation. The training datasets are composed of the combinations of the fault parameters and the resultant thickness and grain size distributions of tsunami deposits. The trained DNN model can estimate the source fault parameters from the measured characteristics of tsunami deposits.

Chapter 3 proposes a new 2D DNN inverse model of tsunami deposits, estimating the source fault model with the homogeneous slip. The model was verified with the measured datasets of the 2011 Tohoku-oki tsunami, which occurred in northeastern Japan. The study area was set at Sendai Plain, Miyagi prefecture. The inverse model was verified with the synthetic data set. Then, the model was applied to the 2011 Tohoku-oki tsunami deposit. Comparison of the predicted fault parameters to the result of other studies verified the applicability of the model to the actual tsunami deposit.

In Chapter 4, the inverse model is developed to estimate the fault model with the heterogeneous slip. In addition to Sendai Plain, the tsunami deposits sampled in Odaka and Rikuzentakata regions were utilized for inversion of the fault parameters. The model was again verified with a synthetic dataset and the 2011 Tohoku-oki tsunami deposit.

Chapter 5 summarizes the conclusions of this thesis and proposes future works.

## **Chapter 2. Methodology**

### **2.1 Introduction**

Several forward models can treat tsunami inundation and sediment transportation, such as TUNAMI-N2 (Goto et al., 1997) with sediment transport model (STM) (Yamashita et al., 2016) and Delft3D-FLOW (Deltares 2021). TUNAMI-N2-STM can treat the transport of sediment composed of a single grain size class, and it was enhanced to calculate the transport of sediment composed of multiple grain size classes (Gusman et al., 2018). However, the current implementation of the non-uniform sediment transport model in TUNAMI-N2-STM lacks consideration of the surface active layer (sediment exchange layer) of bed sediment (Hirano, 1971), which has been considered to be essential for an accurate sediment transport model of multiple grain size classes (Parker, 1991). Thus, the accuracy of TUNAMI-N2-STM is questionable for predicting grain-size sorting in tsunami deposits. Therefore, this study employed Delft3D-FLOW, which can also treat sediment transport of multiple grain size classes.

### **2.2 Forward model of tsunami propagation and sediment transportation**

This study employed Delft3D-FLOW (Deltares, 2021) as a forward model, which has been used for the simulation of the tsunami behavior and transportation of sediment by tsunamis (e.g., Apotsos et al., 2011a, 2011b; Watanabe et al., 2018). It is an open-source software suite including multi-dimensional (2D or 3D) hydrodynamic numerical models with sediment transportation modules. This study used the horizontal 2D hydrodynamic model in Delft3D-FLOW to simulate tsunamis, solving the nonlinear shallow water equations on a two-dimensional staggered grid using a finite difference scheme.

In this model, the water column is approximated as a single layer, and all variables, including velocity or sediment concentration, are depth-averaged. Let  $\xi$  and  $\eta$  be the longitudes and latitudes in the orthogonal curvilinear coordinates, respectively. The fluid mass conservation and momentum conservation equations take the form as follows:

$$\frac{\partial \zeta}{\partial t} + \frac{1}{\sqrt{G_{\xi\xi}\sqrt{G_{\eta\eta}}}} \frac{\partial \left( (d + \zeta)u\sqrt{G_{\eta\eta}} \right)}{\partial \xi} + \frac{1}{\sqrt{G_{\xi\xi}\sqrt{G_{\eta\eta}}}} \frac{\partial \left( (d + \zeta)v\sqrt{G_{\xi\xi}} \right)}{\partial \eta} = 0 \quad (2.1)$$

$$\begin{aligned} \frac{\partial u}{\partial t} + \frac{u}{\sqrt{G_{\xi\xi}}} \frac{\partial u}{\partial \xi} + \frac{v}{\sqrt{G_{\eta\eta}}} \frac{\partial u}{\partial \eta} + \frac{uv}{\sqrt{G_{\xi\xi}\sqrt{G_{\eta\eta}}}} \frac{\partial \sqrt{G_{\xi\xi}}}{\partial \eta} - \frac{u^2}{\sqrt{G_{\xi\xi}\sqrt{G_{\eta\eta}}}} \frac{\partial \sqrt{G_{\eta\eta}}}{\partial \xi} + fv \\ = -\frac{1}{\rho_0\sqrt{G_{\xi\xi}}} P_\xi - \frac{gu\sqrt{u^2 + v^2}}{C_{2D}^2(d + \zeta)} + M_\xi \end{aligned} \quad (2.2)$$

$$\begin{aligned} \frac{\partial v}{\partial t} + \frac{u}{\sqrt{G_{\xi\xi}}} \frac{\partial v}{\partial \xi} + \frac{v}{\sqrt{G_{\eta\eta}}} \frac{\partial v}{\partial \eta} + \frac{uv}{\sqrt{G_{\xi\xi}\sqrt{G_{\eta\eta}}}} \frac{\partial \sqrt{G_{\eta\eta}}}{\partial \xi} - \frac{v^2}{\sqrt{G_{\xi\xi}\sqrt{G_{\eta\eta}}}} \frac{\partial \sqrt{G_{\xi\xi}}}{\partial \eta} + fu \\ = -\frac{1}{\rho_0\sqrt{G_{\eta\eta}}} P_\eta - \frac{gv\sqrt{u^2 + v^2}}{C_{2D}^2(d + \zeta)} + M_\eta \end{aligned} \quad (2.3)$$

where  $u$  and  $v$  indicate the depth-averaged velocities on an orthogonal curvilinear grid for  $\xi$  and  $\eta$  direction, and  $d$  denotes depth below the datum. The parameter  $\zeta$  is the water level above the datum,  $g$  is the acceleration due to gravity, and  $\rho_0$  denotes the density of water.  $P$  is water pressure,  $C_{2D}$  is the 2D Chezy coefficient, and  $M$  is the contribution due to external forces or sinks of momentum. This model considers coordinate transformation from curvilinear to rectangular coordinates, which is significant in the case of large calculation domains.  $G_{\xi\xi}$  and  $G_{\eta\eta}$  are coefficients to transform curvilinear to rectangular coordinates, and  $f$  is the Coriolis parameter (inertial frequency).

The sediment transport model considers both suspended load and bedload, which are defined as sediment transport above and below the reference height  $a$  (Van Rijn, 1993). The transfer of sediment between the bed and the flow is modeled on the near-bottom layer that is entirely below the reference height, which is referred to as the active layer. The suspended sediment concentration  $C_a$  at the reference height is calculated using

the following equation.

$$C_a = f_{SUS} 0.015 \rho_s \frac{D_{50} (T_a)^{1.5}}{a (D_*)^{0.3}} \quad (2.4)$$

where  $f_{SUS}$  denotes a factor for suspended sediment transport by a current, and  $\rho_s$  is the specific density of sediment.  $D_{50}$  is the median diameter of the sediment, and  $T_a$  denotes the non-dimensional bed shear stress. The parameter  $D_*$  is the non-dimensional particle diameter.

The concentration at the bottom of the active layer  $C_{kmx}$  is calculated assuming a standard Rouse profile between the reference level  $a$  and the center of the active layer as follows:

$$C_{kmx} = C_a \left( \frac{a(h - z_{kmx})}{z_{kmx}(h - a)} \right)^A \quad (2.5)$$

where  $h$  is water depth, and  $z_{kmx}$  denotes the elevation of the center of the active layer.  $A$  represents the Rouse number.

The settling velocity of the sand fraction was calculated based on the Van Rijn (1993) method, depending on grain size. For the grain size range used in this study (0.1–2.0 mm), settling velocity ( $w_s$ ) is computed in equation 2.6.

$$w_s = \frac{10\nu}{D_s} \left( \sqrt{1 + \frac{0.01(s-1)gD_s}{\nu^2}} - 1 \right) \quad (2.6)$$

where  $s$  is the relative density of sediment,  $D_s$  is the representative diameter of sediment, and  $\nu$  is the kinematic viscosity coefficient of water.

The entrainment flux  $E$  from sediment through the active layer is expressed in equation 2.7.

$$E = a_2 \varepsilon_s \left( \frac{C_a - C_{kmx}}{\Delta z} \right) \quad (2.7)$$

where  $a_2$  is a correlation factor for sediment concentration, and  $\varepsilon_s$  denotes the sediment diffusion coefficient evaluated at the bottom of the active layer. The parameter  $\Delta z$

represents a difference in elevation between the center of the active layer and reference height.

The settling flux of sediment particles  $D$  through the bottom of the active layer is given as follows:

$$D = w_s C_{kmx} \quad (2.8)$$

Bedload transport is shown in equation 2.9.

$$q_b = f_{BED} 0.006 \rho_s \omega_s D_s m^{0.5} m_e^{0.7} \quad (2.9)$$

where  $f_{BED}$  is a factor for sediment transport by bedload,  $\rho_s$  is the specific density of sediment fraction,  $D_s$  is the representative diameter of sediment (Van Rijn, 1993), and  $m$  and  $m_e$  are the sediment mobility number and the excess sediment mobility number, respectively. The parameters  $m$  and  $m_e$  were calculated by following equations.

$$m = \frac{v^2}{(s-1)gD_{50}} \quad (2.10)$$

$$m_e = \frac{(v - v_{cr})^2}{(s-1)gD_{50}} \quad (2.11)$$

where  $v$  is the depth-averaged velocity,  $D_{50}$  is the median diameter of sediment. The parameters  $v_{cr}$  and  $s$  represent the critical depth-averaged velocity for incipient motion and the relative density of sediment, respectively.

Critical bed shear velocity is shown in equation 2.12.

$$u_{*,cr}^2 = g\Delta D_{50}\theta_c \quad (2.12)$$

where  $\theta_c$  is the Shields parameter. Sediment transportation occurs when the bed shear velocity exceeds the critical bed shear velocity.

In this study, the distribution of grain size diameter was discretized into four classes (0.14 mm, 0.25 mm, 0.42 mm, 1.00 mm). Volume per unit area of each grain size class is calculated at the smallest domain for each region (see details in Chapters 3 and 4). Manning's roughness coefficient at each grid was set according to the land condition.

Following Sugawara et al. (2014), a roughness coefficient of 0.025 was assigned for water, 0.03 for bare ground, and 0.05 for residential areas.

This study set six nested calculation domains to calculate the tsunami wave propagation using Delft3D-FLOW. The spatial grid size for each region is 3645 m, 1215 m, 405 m, 135 m, 45 m, and 15 m from Domains 1 to 6. The time step was 0.3 sec for all calculation domains.

The fault model determining sea-bottom and surface deformation was calculated using the method of Okada (1985). This method requires the northeast edge of fault location, fault depth, strike, dip, rake, length, width, and fault slip as initial fault parameters.

### **2.3 Inverse model for tsunami deposit using DNN**

The inverse model aiming at the reconstruction of the fault parameters and source sediment properties was constructed by a DNN. The artificial training dataset produced by the forward model calculation was used to train the DNN to develop the inverse model estimating the fault parameters from the depositional characteristics. Mitra et al. (2020) proposed this inverse modeling framework, which employed a 1D forward model. The present study improved the method to estimate the fault parameters using a 2D forward model.

The neural network used in this study was composed of the input layer, three hidden layers composed of 1000 nodes, and the output layer (Fig. 2-1). The input layer accepts the values of volume-per-unit areas of four grain-size classes at each sampling point. The output layer was composed of 6 nodes (Chapter 3) or 16 nodes (Chapter 4) that provided the estimates of initial fault parameters and sediment parameters.

The training data for the inverse model is prepared by using the forward model.

Multiple initial fault conditions, such as fault slip and width (Chapter 2), fault length, width, and locations (Chapter 3), are generated randomly with a range of possible values in the natural environment. Then, the forward model calculated tsunami propagation and sediment transportation in the study area to obtain the thickness and unit per volume of each grain size of tsunami deposits. Then, the result of the forward model was given to an input layer of DNN. It should be noted that the normalization of the input and teacher values was performed. After this normalization, all parameters and input values ranged from 0 to 1. This study used the rectified linear activation function (ReLU) as an activation function following the previous studies (Mitra et al., 2020, 2021; Naruse and Nakao, 2021). The 50 % dropout was applied to all nodes in the hidden layers. The output of the inverse model was evaluated using the loss function defined in equation 2.13 (Mitra et al., 2020).

$$J = \frac{1}{N} \sum (I_k^{fm} - I_k^{NN})^2 \quad (2.13)$$

where  $I_k^{fm}$  denotes a ground-truth parameter used to produce the  $k$ th training data and  $I_k^{NN}$  is the corresponding predicted parameter by the DNN.

The stochastic gradient descent method (SGD) was used to optimize the weight coefficients of DNN to minimize the loss function. The Nesterov momentum method was used with the momentum parameter 0.9. The hyperparameters for the learning procedure in this study were the learning rates, batch size, and number of epochs. These are set as follows by trial and error. The batch size was set to 32, and the learning rate was 0.02. The number of training epochs was 10000. The inverse model was implemented using Python 3.7.3 with the Numpy, Scipy, and TensorFlow 2.4 packages.

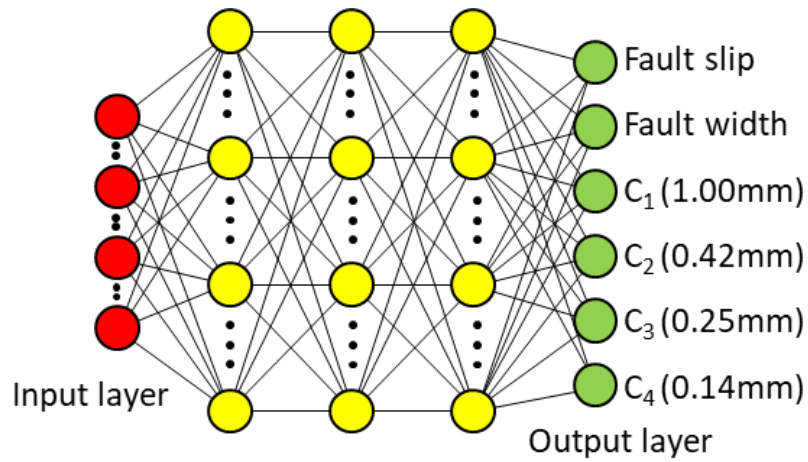


Fig. 2-1. Neural network architecture for the inverse model used in Chapter 3.

## 2.4 Summary

This chapter explained the forward and inverse models used in this study.

Delft3D-FLOW was utilized as the forward model in this study. The model solves the nonlinear shallow water equations on a two-dimensional staggered grid using a finite difference scheme to predict the dynamics of tsunami propagation. The sediment transport models for suspended load and bedload were included in this forward model.

The inverse model based on DNN was chosen for this study. Although previous studies proposed this inverse modeling framework, they employed the 1D forward model as training data. This study improved the method to estimate the fault parameters using a 2D forward model.

## **Chapter 3. Reconstruction of fault parameters from tsunami deposits**

### **3.1 Introduction**

The 2011 off the Pacific coast of Tohoku Earthquake Tsunami (hereafter referred to as the 2011 Tohoku-oki tsunami) caused severe damage along the Pacific coast of northeastern Japan (Fire and Disaster Management Agency, 2020). Historical and geological records indicate that this region has repeatedly suffered from tsunamis (Goto et al., 2021). Among these tsunami events, some were estimated to have originated from the Japan Trench as subduction zone earthquakes, e.g., the 869 Jogan tsunami (Satake et al., 2008; Namegaya et al., 2010) and the 1611 Keicho tsunami (Hatori, 2009). However, these estimations were based on only the similarity between the distribution of the tsunami deposit and the tsunami inundation areas. Note that similarity in terms of both the extent and displacement of the source fault should be considered to discuss the recurrence cycle of earthquakes; however, such data are typically not available for previous tsunamis.

Accurate estimation of fault parameters of tsunami sources is essential for effective tsunami risk assessment. Complex tsunami behavior can be predicted from the fault parameters of the wave source using the forward model calculation (e.g., Satake et al., 2013); thus, assessing the fault parameters of repeated large tsunamis contributes to disaster prevention planning. However, data on tsunami characteristics (e.g., wave height and inundation areas), which is used in the current estimation method (e.g., Imamura et al., 2012; Satake et al., 2013), are not available for past tsunamis. Therefore, tsunami deposits are essential sources of information that facilitate the reconstruction of the scale of past tsunamis. The inverse methods for tsunami deposits proposed to date tend to oversimplify the hydraulic conditions and do not reproduce the complex behavior of the

actual tsunami adequately. It was pointed out that these methods tend to overestimate or underestimate the scale of the flow when verified against known recent tsunami events (Sugawara et al., 2014).

Thus, this study proposes an inverse analysis method to reconstruct the source fault parameters from tsunami deposits using a 2D layer-averaged model and a DNN. The proposed method utilizes a 2D forward model, i.e., Delft3D-FLOW (Deltares, 2021), which can account for tsunami behaviors on complex geometry and the deposition of sediment of mixed grain size (Watanabe et al., 2018). In previous studies, the DNN inversion method has been employed to estimate the flow conditions using the 1D forward model (Mitra et al., 2020, 2021; Naruse and Nakao, 2021) under the assumption of a flat topography. In this inverse modeling process, the forward model calculation was repeated with various initial parameters to produce datasets of thickness and grain size distributions of onshore tsunami deposits. Subsequently, the DNN inverse model was trained to learn the relationship between the initial model parameters and the depositional characteristics. The trained model was then applied to actual tsunami deposits of the 2011 Tohoku-oki and the 2004 Indian Ocean tsunamis to predict reasonable values for the tsunami hydraulic conditions (Mitra et al., 2020, 2021). However, differing from previous studies, the proposed inverse model attempts to estimate the source fault characteristics directly from tsunami deposits rather than the local hydraulic conditions of the tsunami inundation flows.

## **3.2 Method**

### **3.2.1 Forward model for tsunami propagation and sediment transportation**

In this study, we used the Delft3D-FLOW (Deltares, 2021) as the forward model, which has been used to simulate tsunamis and the transportation of sediments by tsunamis (Apostsos et al., 2011a, 2011b; Watanabe et al., 2018). This model solves the horizontal 2D shallow water equations to predict the tsunami propagation dynamics. Regarding sediment transport modeling, the bedload and suspended load, which are defined as the sediment transport below and above the reference height, respectively, were calculated using the formulation proposed by Van Rijn (1993).

The target area for analysis is the right bank of the Nanakita River in Sendai City, Miyagi Prefecture, Japan (Fig. 3-1), where the 2011 Tohoku-oki tsunami deposit was investigated three months after the event (Abe et al., 2012; Naruse and Abe, 2017). The thickness and grain size distribution of the tsunami deposit were obtained along the transect established perpendicular to the shoreline (Fig. 3-1).

The topographic data were based on a 5-m mesh digital elevation model provided by the Geospatial Information Authority of Japan that was constructed prior to the 2011 Tohoku-oki earthquake. The computational domains followed the scheme reported by Watanabe et al. (2018), which comprises six nested domains (Fig. 3-1). Domain 1, which contains the Japan Trench and the entire northeast region of Japan, covered the most extensive region among all domains. In contrast, Domain 6 covered the smallest region, including the northern part of Sendai Plain, south of the Nanakita River, Miyagi Prefecture, Japan (Fig. 3-1). Note that the sediment transport was calculated only in Domain 6. The spatial grid size for each region was 3645 m, 1215 m, 405 m, 135 m, 45

m, and 15 m from Domain 1 to Domain 6. The time step was 0.3 s for all calculation domains. The source area of the tsunami deposit was set as the region over the seabed, beach, and aeolian dunes, following the estimation presented by Sugawara et al. (2014). The grain size distribution of the surface sediment in the source area was discretized into four-grain size classes (1.00, 0.42, 0.25, and 0.14 mm) to cover the grain size distribution of the tsunami deposit observed in this area (Naruse and Abe, 2017). Here, we assumed that the grain size distribution was spatially uniform in the source area, whereas a fraction of each grain size class was subject to be estimated by the inverse analysis.

Two fault parameters, i.e., the amount of fault slip and fault width, were generated randomly from 1–40 m and 10–200 km (Fig. 3-2). Other fault parameters (i.e., the fault length, strike, dip, and rake) were determined following Imamura et al. (2012). Although the length along the trench axis of the fault is uncertain, the fault length was set to 500 km, which is the same value as the previous study (Imamura et al., 2012), because the earthquake was assumed to be one of the largest in history. One random number for each grain size class was generated within the same range, and the fraction of bottom sediment in the source area for each grain size class was set as a value normalized by the sum of those random numbers.

Given these six initial parameters, the forward model calculated the propagation of the tsunami wave from Domains 1 to 6, and the amount of sediment accumulation for each grain size class was computed in Domain 6. The volume per unit area of each grain size class was then obtained at the 35 sampling points along the transect perpendicular to the shoreline (Fig. 3-1). The locations of the sampling points were set at those surveyed by Naruse and Abe (2017).

The forward model calculation was repeated 1500 times with randomly

generated initial parameters. As a result of iterating the calculation, the combinations of the six initial parameters and the resultant volumes per unit area of four grain size classes of the tsunami deposit at the sampling points were obtained, which were then used to train and validate the proposed inverse model, which is discussed in the following section.

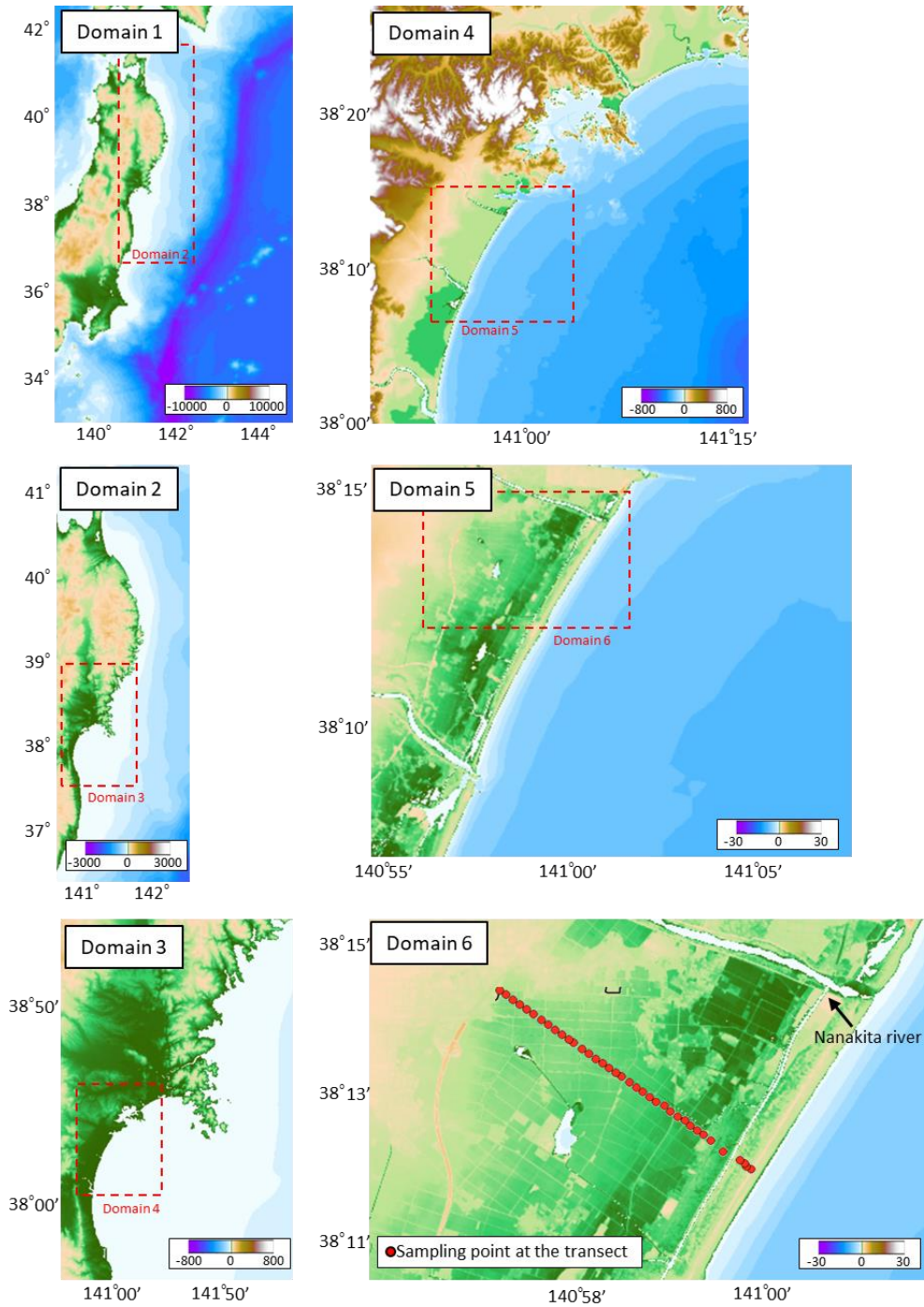


Fig. 3-1. Bathymetry data and domains used for forward model. The red dashed box of each domain indicates the smaller domain in the nesting grid system. Domain 1 covers the entire northeastern area of Japan and the Japan Trench, while Domain 6 is the smallest domain, which covers Sendai Plain. The transect used for the output of the forward model is shown in Domain 6.

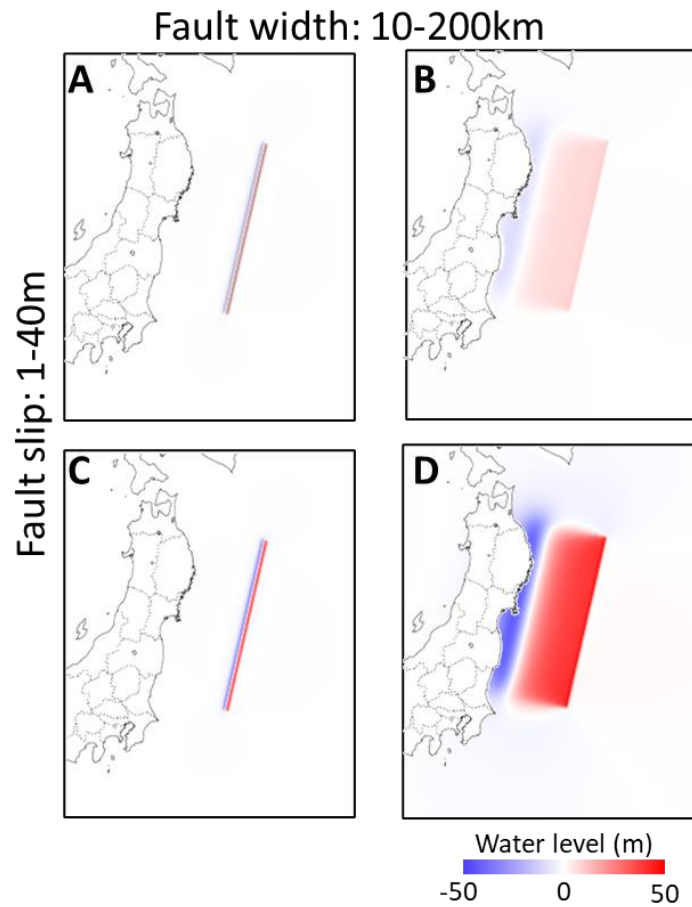


Fig. 3-2. Example of initial fault model as input for forward model. Fault slip and width for each figure are (A) slip:1 m, width: 10 km, (B) slip: 1 m, width: 200 km, (C) slip: 40 m, width: 10 km, (D) slip: 40 m, width: 200 km.

### 3.2.2 Inverse model using deep neural network

The inverse model used to reconstruct the fault parameters and source sediment properties was constructed using a DNN. Here, the artificial training dataset produced by the forward model calculation was used to train the DNN to develop an inverse model to estimate the relevant fault parameters from the depositional characteristics. Mitra et al. (2020) proposed this inverse modeling framework, which employed a 1D forward model. The current study improved the method to estimate the fault parameters using a 2D forward model.

The DNN used in this study comprised an input layer, three hidden layers composed of 1000 nodes, and an output layer (Fig. 2-1). The input layer takes the values of the volume per unit areas of four grain size classes at 35 sampling points as input; thus, the input layer comprised 140 nodes. The output layer comprised six nodes that provided the estimates of the initial fault and sediment parameters (i.e., fault width, slip, and fractions of the four grain size classes of the source sediment).

The inverse model was trained on an artificial dataset obtained via iteration of the forward model calculation. The output of the inverse model was evaluated using the following loss function (Mitra et al., 2020):

$$J = \frac{1}{N} \sum (I_k^{fm} - I_k^{NN})^2 \quad (3.1)$$

where  $I_k^{fm}$  denotes the ground-truth parameters used to produce the  $k$ th training data, and  $I_k^{NN}$  is the predicted parameters by the DNN model.

Here, the stochastic gradient descent method was used to optimize the weight coefficients of the DNN to minimize the loss function. The Nesterov momentum method was used with the momentum parameter 0.9. The tuned hyperparameters included the learning rates, batch size, and the number of epochs, which were set by trial and error. The batch size, learning rate, and number of training epochs were set to 32, 0.02, and 10000, respectively.

The DNN model was trained on an artificial dataset comprising 1400 cases, which was split into a training set (80%) and a validation set (20%). Note that cases where the run-up distances were less than 350 m from the shoreline were excluded from the training datasets because tsunamis of small magnitude leave little or no sediment. In addition, the preservation potential of deposits near shorelines is low in tsunami deposits; thus, this study only considered large-scale tsunamis that inundate inland regions.

### **3.2.3 Jackknife error estimation**

The precision of the inversion result was evaluated using the Jackknife method (Quenouille, 1949; Mitra et al., 2020). In this study, there were 35 output points from the forward model along the transect. Using the Jackknife method, one of the 35 output points was omitted, and then we conducted training and inverse analysis of the 2011 Tohoku-oki tsunami deposit to estimate the pseudo-values of the fault parameters and the initial percentage of the four-grain size classes. This process was repeated 35 times, resulting in 35 results of inversion without one output point. Then, the estimate of the standard error from the variance of the pseudo-values was obtained.

### **3.3 Result**

#### **3.3.1 Training of inverse model and validation with synthetic data**

The proposed DNN inverse model to estimate the fault parameters from tsunami deposits was trained on the artificial dataset of 1400 cases of the forward model calculation. The training results demonstrated that the loss function values for the training and validation datasets exhibited no significant deviation, which indicates that no overlearning occurred in the training process (Fig. 3-3). The relationship between the loss function values and the number of training datasets (Fig. 3-4) indicated that the training result improved as the number of training datasets increased to 700. However, increasing the number of training datasets beyond 800 did not yield remarkable model performance improvements; thus, 1400 sets of artificial training data are considered sufficient for the proposed DNN inverse model.

Following the training phase, the model was tested on 100 artificial datasets to confirm the model's performance on unseen datasets. We found that the predicted fault parameters well-matched the ground truth values of the test datasets (Fig. 3-5), as well as the predicted grain size distribution (Fig. 3-6). Here, the root mean squared error (RMSE) values of the fault slip and width were 2.41 m and 5.18 km.

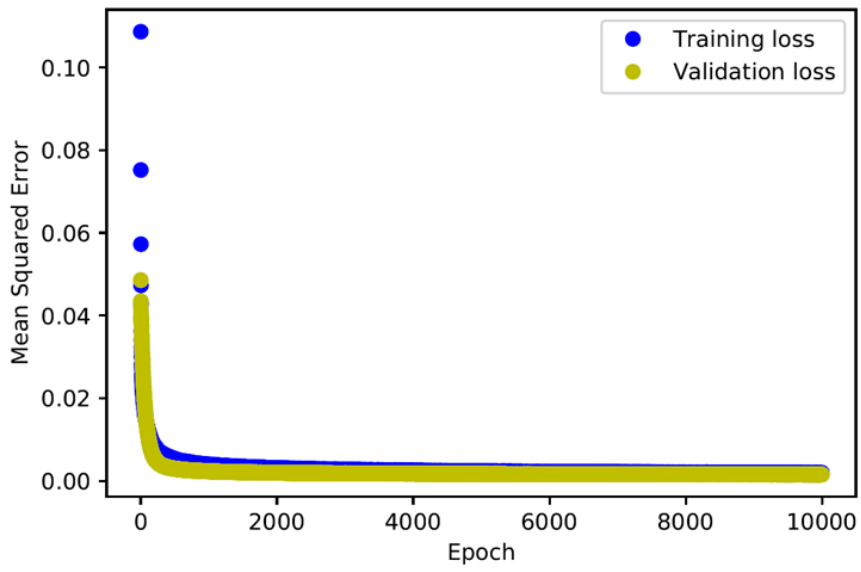


Fig. 3-3. Learning history of the inverse model on artificial datasets.

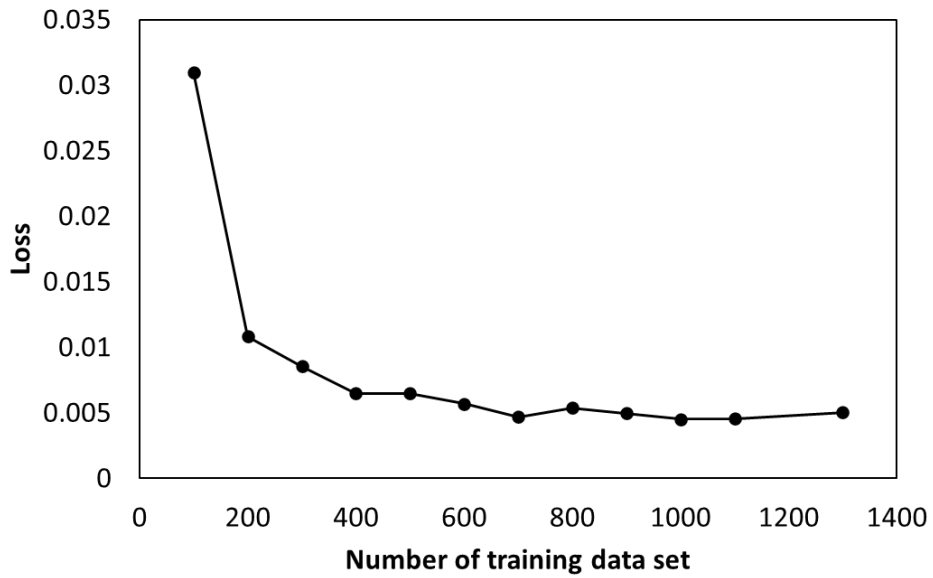


Fig. 3-4. Relationship between number of training datasets and the value of loss function.

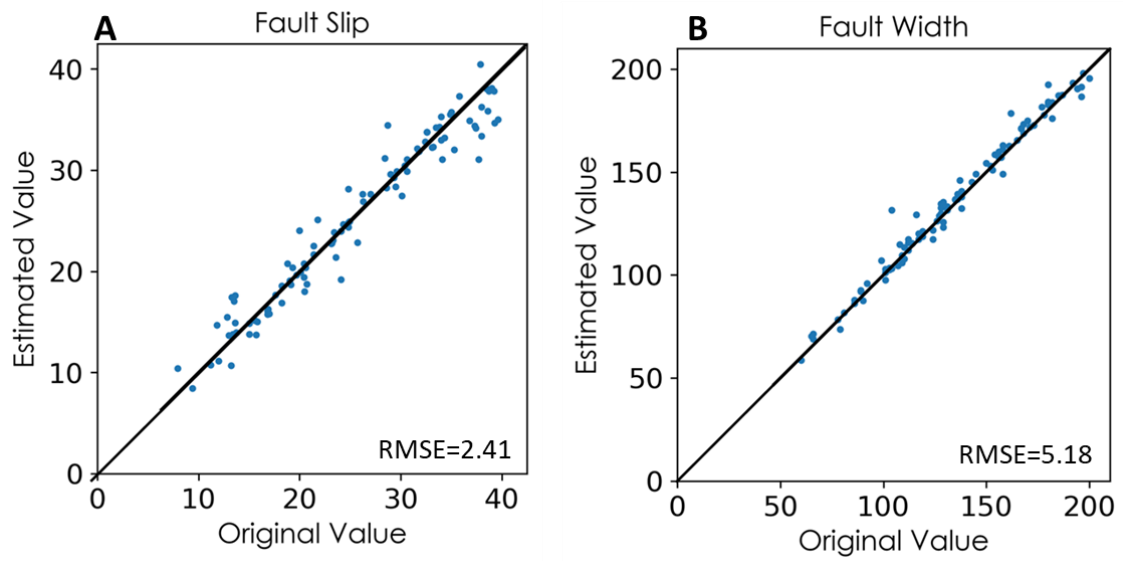


Fig. 3-5. Results of the model test for (A) fault slip and (B) width. The plot with the predicted value obtained by inverse model against the original values was distributed along the 45-degree line, which indicates that the measured and estimated values of the inverse model correspond well.

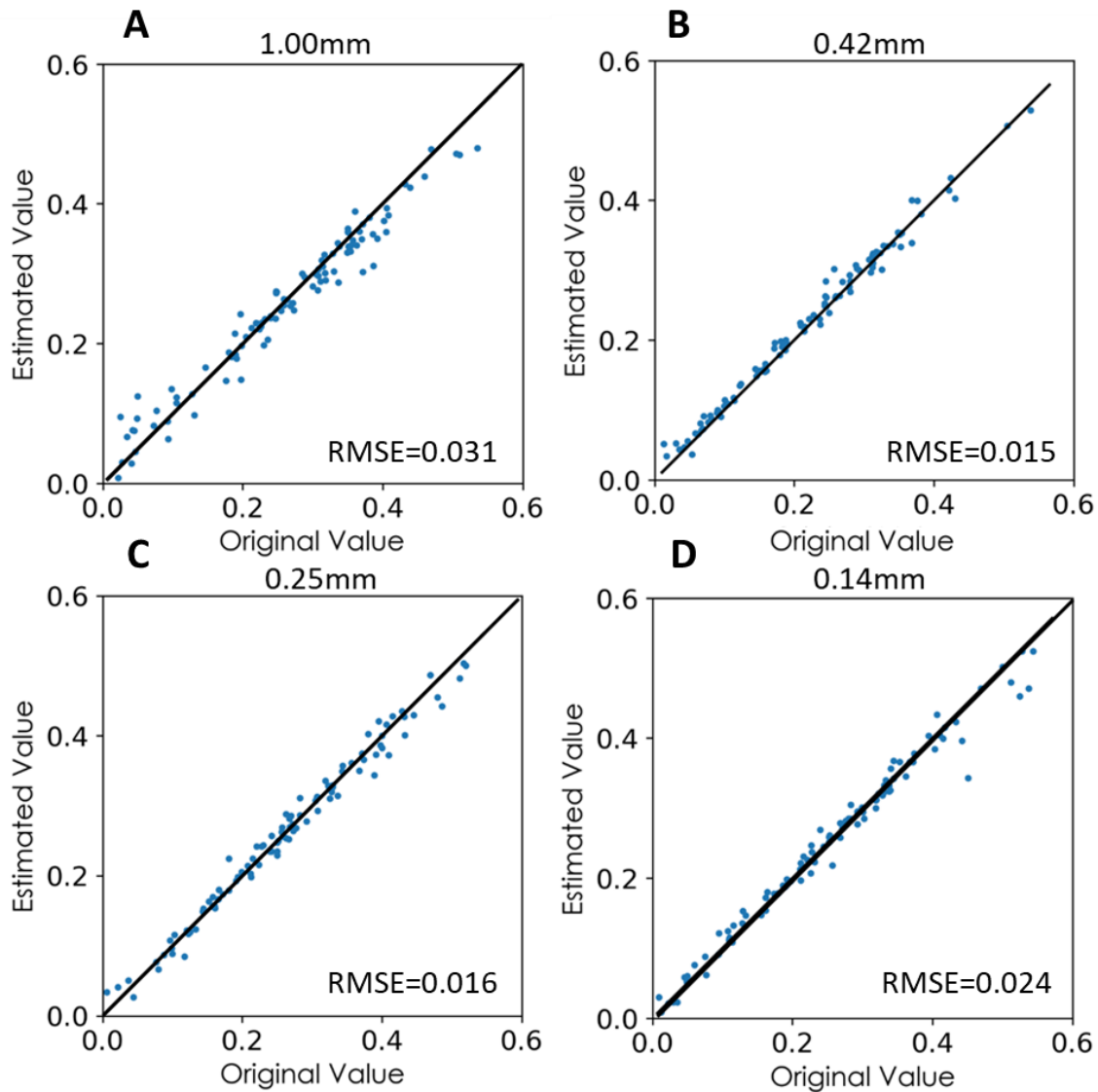


Fig. 3-6. Result of validation with synthetic data set for four-grain size classes (A: 1.00 mm, B: 0.42 mm, C: 0.25 mm, D: 0.14 mm).

### 3.3.2 Inverse analysis of the 2011 Tohoku-oki tsunami and error estimation

The inverse model was applied to the tsunami deposit formed by the 2011 Tohoku-oki tsunami. Here, the fault slip and width were estimated as 21.3 m and 119.9 km, respectively (Table 3-1), and the 95% confidence intervals in Jackknife tests for the estimated fault slip and width values were 0.47 m and 1.30 km, respectively (Table 3-1, Fig. 3-7).

Fig. 3-8 compares the estimated coseismic slip against the distance to the Japan Trench of the 2011 Tohoku-oki tsunami with fault models of past studies (Lay, 2018). Based on the results reported by previous studies (Imamura et al., 2012; Ozawa et al., 2012; Satake et al., 2013; Melgar and Bock, 2015), the coseismic slip ranges from 10–40 km at 0–50 km from the trench axis; however, it decreases rapidly toward the island arc, and the displacement decreases to 0–15 m at 130 km from the trench axis. Note that these estimates are consistent with the inversion results obtained by the proposed model (Fig. 3-8).

The moment magnitude of the earthquake ( $M_w$ ) was calculated as 8.9 from the fault area estimated in this study with the following equation (The Headquarters for Earthquake Research Promotion, 2017).

$$M_0 = 16/(7\pi^{3/2}) \cdot \Delta\sigma \cdot S^{3/2} \quad (3.2)$$

$$M_w = \frac{2}{3} \log M_0 + 6.07 \quad (3.3)$$

where  $M_0$  is the moment,  $\Delta\sigma$  is an average stress drop, which was estimated to be 4.3 (Fujiwara et al., 2015), and  $S$  is the fault area. The calculated value was very close to the values of  $M_w$  9.0–9.1 estimated in the previous seismological studies (Lay, 2018).

The estimated grain size distribution in the sediment source area is shown in Table 3-1. It should be noted that the sum of the percentages of all grain size classes does not necessarily equal 100 % because each percentage is estimated independently by the proposed DNN. The sediment grain size in the coastal source area, such as dunes and sea beds, was reported to be 1.5–2.4 phi (0.35–0.19 mm) and 1.2–2.4 phi (0.43–0.18 mm) (Matsumoto, 1985). Using the proposed inverse model, we found that the 0.25-mm grain size class was the most dominant (71%), followed by the 0.42-mm class (19%), and these results correspond well to the grain size measured at the source area.

Table 3-1. Estimated fault parameters and initial percentage of sediment from inverse analysis. The Jackknife error estimation results are also shown.

Parameter	Predicted results	Jackknife error
Fault slip (m)	21.3	$\pm 0.47$
Fault width (km)	119.9	$\pm 1.30$
1.00 mm (%)	3.9	$\pm 0.35$
0.42 mm (%)	19.6	$\pm 0.16$
0.25 mm (%)	71.0	$\pm 0.47$
0.14 mm (%)	3.6	$\pm 0.18$

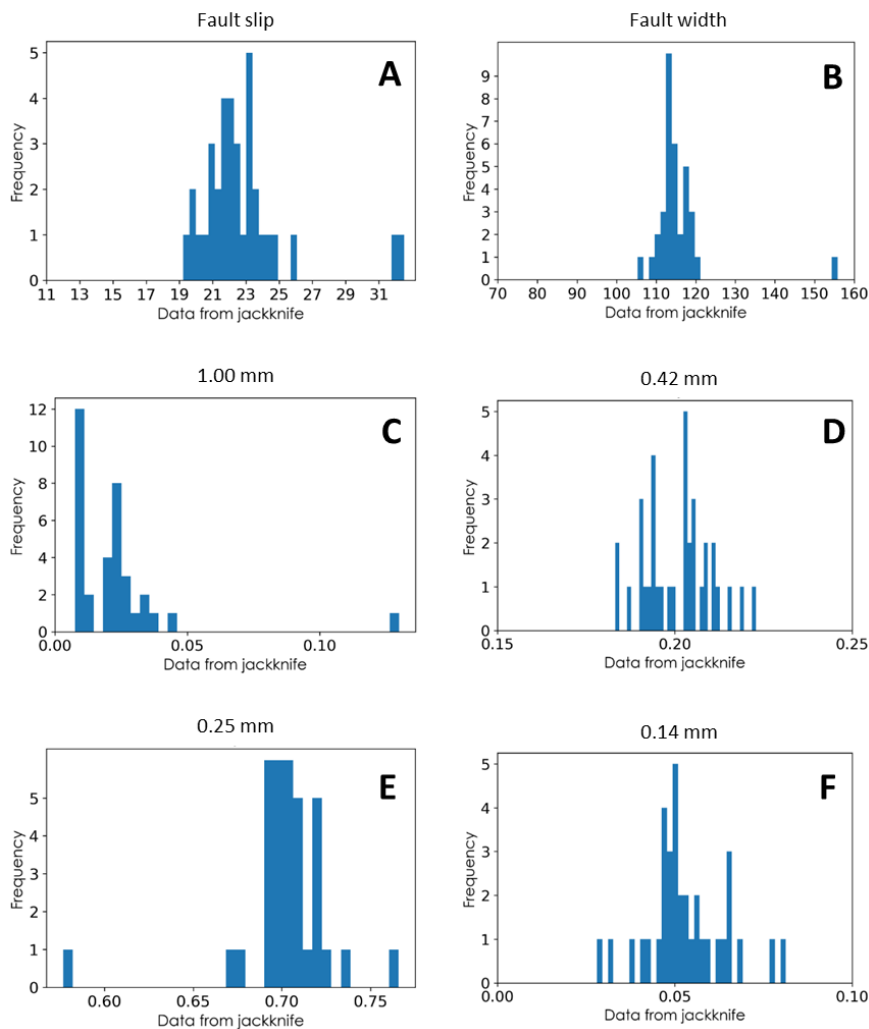


Fig. 3-7. Histogram of pseudo-value obtained through Jackknife error estimation (A: Fault slip, B: Fault width, C: Grain size of 1.00 mm, D: Grain size of 0.42 mm, E: Grain size of 0.25 mm, F: Grain size of 0.14 mm).

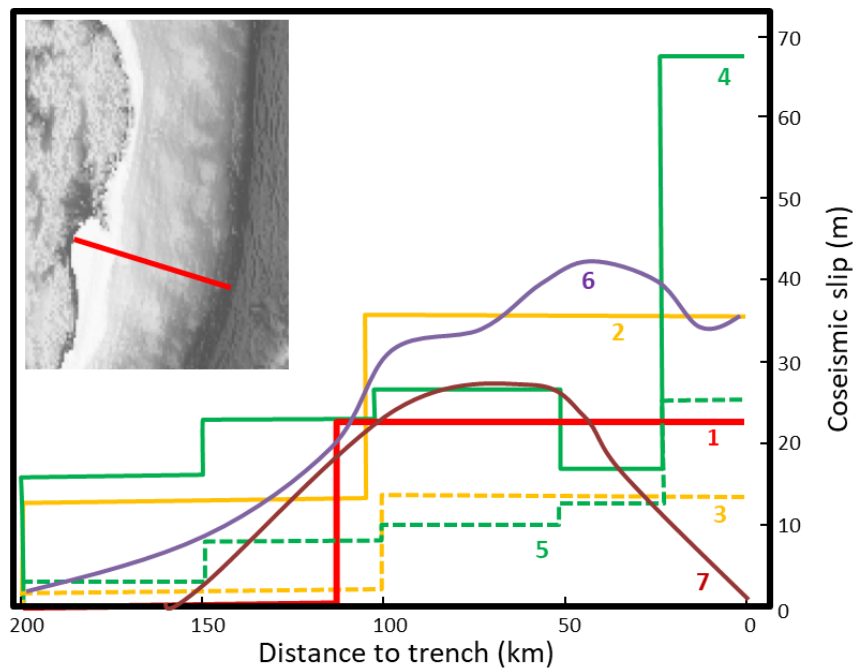


Fig. 3-8. Comparison of the proposed and previous fault models. The coseismic slip against the distance to the trench is shown. The number of each line is identified as follows. 1: This study; 2: Imamura et al., 2012; 3: Average of Imamura et al., 2012; 4: Satake et al., 2013; 5: Average of Satake et al., 2013; 6: Melgar and Bock, 2015; 7: Ozawa et al., 2012. It should be noted that lines 3 and 5 were obtained by averaging the slip of each segment for the north-south direction.

### 3.3.3 Estimated behavior of the tsunami inundation flow and depositional features

The forward model calculation was conducted using the estimated initial parameters to obtain the deposit thickness, the volume per unit area of each grain size class, and the hydraulic properties of the tsunami in the study area. Figs. 3-9A and 3-9B shows the spatial distribution of the measured and estimated thickness values of the tsunami deposit. Although the calculated results approximate the measured values well, a slight difference was observed in the landward region approximately 3000 m from the shoreline. Figs. 3-9C to 3-9F show the calculated and measured volume per unit area value for each grain size class of the tsunami deposit along the transect. As shown, the calculated volumes

also match the measured value for all grain size classes, although differences were observed in the region approximately 3000 m from the shoreline, where measured volume per unit area decreased rapidly.

The tsunami flow characteristics were reconstructed well (Fig. 3-10). The inundation flow velocity measured 7 km south from the transect was close to the estimated values, especially in the region 1000–1500 m from the shoreline. In addition, the calculated inundation heights matched the maximum inundation heights measured at the sites in the study area, although they were slightly (0.5–1.0 m) overestimated at the inland area.

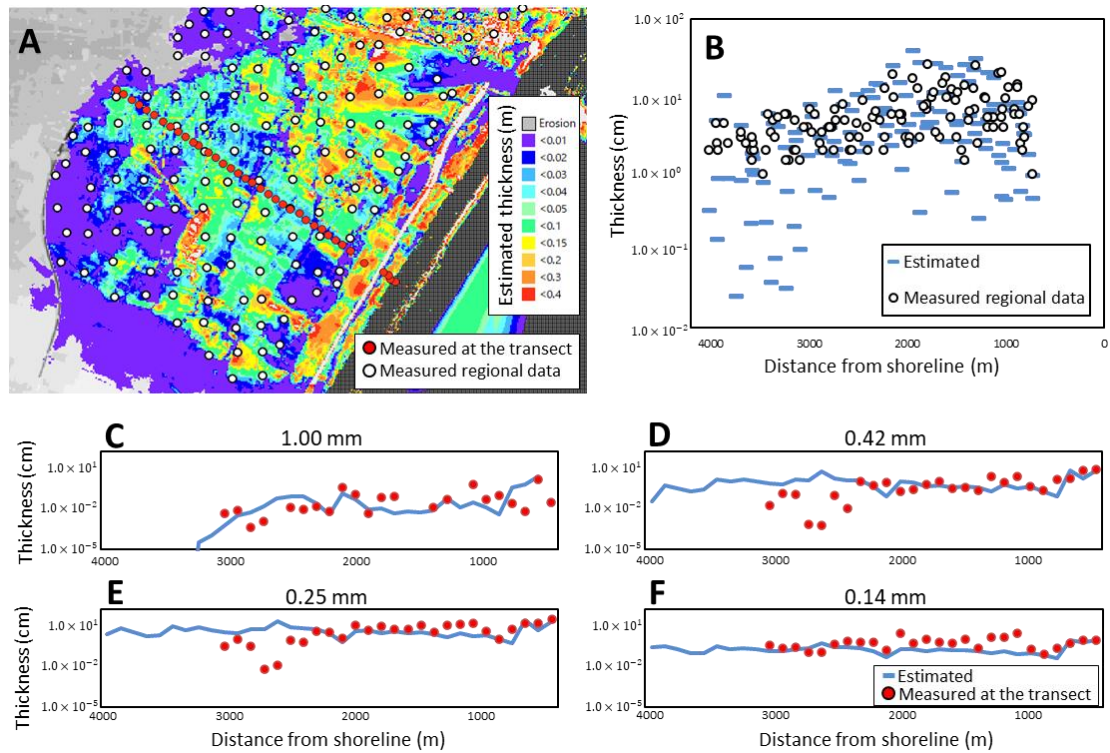


Fig.3-9. Comparison of estimated and measured thickness of tsunami deposit. (A) Spatial thickness of bulk tsunami deposit calculated by the forward model. Here, the red dots show the sampling point locations for the transect, and the white dots are the locations of the sampling point for the measured regional data obtained by Miyagi Prefecture/Mirodi-net Miyagi and presented in Goto et al. (2012). (B) Comparison of estimated and measured thickness values of bulk tsunami deposits. The white dots are the measured thickness values of the bulk tsunami deposit, and the blue bar is the bulk thickness calculated by the forward model at the same point the bulk tsunami deposit thickness was measured. Here, the initial parameter estimated by the inverse model was used. Comparison of estimated and measured thickness of tsunami deposit for (C) 1.00-mm, (D) 0.42-mm, (E) 0.25-mm, and (F) 0.14-mm grain size classes.

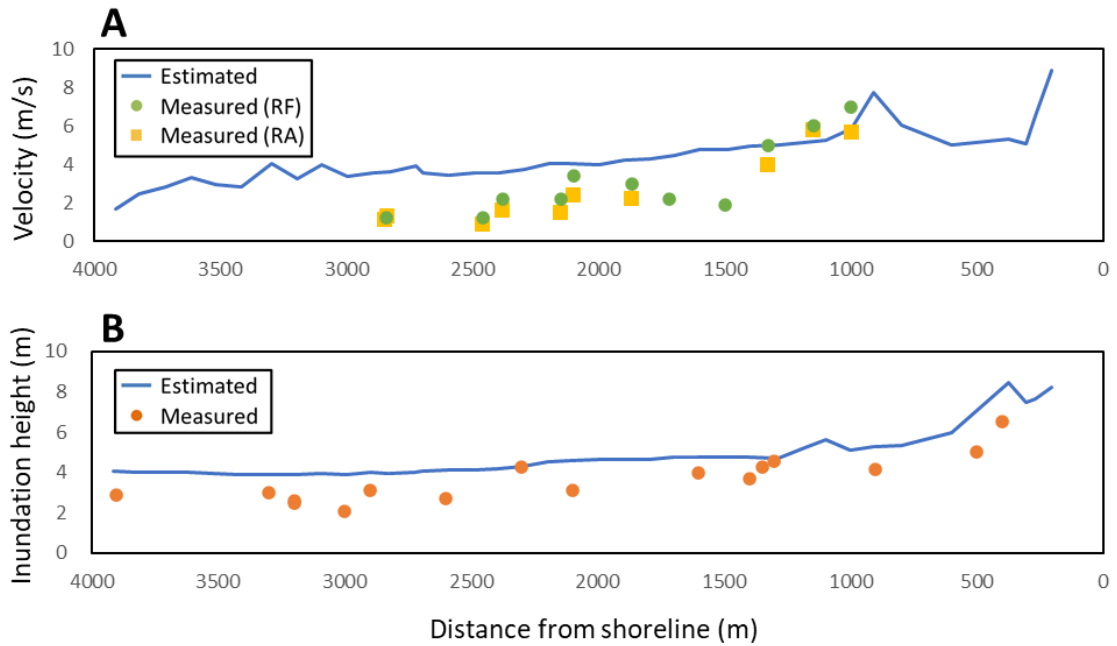


Fig. 3-10. Comparison of estimated and measured flow information of tsunami values. (A) Measured and estimated velocity at the wavefront of inundating tsunami. RF denotes the velocity measured at a rice field, and RA denotes that of a residential area. Note that the velocity was measured 7 km south of the transect because velocity is not typically measured along the transect. (B) Measured and estimated inundation height above Tokyo Peli along the transect. The maximum inundation height value corresponds well to the estimated value.

## **3.4 Discussion**

### **3.4.1 Reconstructed fault parameters of the 2011 Tohoku-oki tsunami deposit**

The proposed DNN-based inverse model of tsunami deposits reconstructed reasonable values for the wave source fault parameters and the inundation flow behaviors based on an exhaustive examination of the fault parameters from the depositional information, whereas few attempts have been made to reconstruct fault parameters solely from tsunami deposits in previous studies (Satake et al., 2008; Sugawara et al., 2011). Previous studies did not search exhaustively for possible fault parameters. In this study, the estimated distribution of slip displacement and moment magnitude of the earthquake was consistent with the compilation study of the 2011 Tohoku-oki tsunami (Lay, 2018). implying that information on initial fault parameters selected for this study was preserved as the features of the thickness and grain size distribution of the tsunami deposit.

### **3.4.2 Advantage of proposed 2D inverse model for tsunami deposits and future challenges**

In this study, we developed a DNN-based inverse model to estimate fault parameters from tsunami deposits. The proposed model is applicable to complicated topographies and can be used to estimate the wave source fault parameters directly. It was found that the proposed method reconstructed the hydraulic conditions of the 2011 Tohoku-oki tsunami precisely. Previous inverse models of tsunami deposits can only reconstruct tsunami characteristics onshore, assuming a flat topography and applying a highly simplified hydraulic situation (Jaffe and Gelfenbuam, 2007; Naruse and Abe, 2017; Mitra et al., 2020).

The findings of the current study indicate that it is possible to estimate past earthquakes and tsunamis over a wide area, even if the survey is concentrated in a

particular region. This study has demonstrated that the width and slip, i.e., the moment magnitude of the along-trench earthquake, can be estimated using only tsunami deposits in a specific area (the Sendai Plain was the target considered in the current study). Subsequently, the velocity and inundation depth of the tsunami were reconstructed adequately from wave source fault information. Note that paleo-tsunami deposits are not always found along specific transects; however, the development from the 1D model to the 2D forward model in this study enabled effective reconstruction from a limited number of study sites scattered across more complex topography. The inundation heights of past tsunamis estimated by the proposed inverse analysis method are expected to contribute to the design of effective disaster prevention facilities.

Reconstruction of more detailed features of the source fault, e.g., the variation in displacement over multiple fault segments, will likely require information on tsunami deposits at several remote regions. In addition, estimating the uneven displacement distribution of past trench earthquakes is essential to model the periodicity of trench earthquakes (Seno, 2012) and estimate intra-plate or outer-rise earthquakes (Abe, 1978), which will be the focus of future research.

### **3.5 Conclusions**

This study proposed a new inverse model to estimate the fault parameters of the tsunami source directly from tsunami deposits. The model utilized the DNN, which is trained by artificial datasets produced by the forward model of tsunami propagation and sediment transportation. The inverse model was validated with synthetic datasets, and the model successfully reconstructed initial fault parameters from properties of tsunami deposits with high accuracy. Then, we performed an inverse analysis of actual data from the 2011 Tohoku-oki tsunami deposit to test the applicability of the inverse model in natural cases.

The model predicted a fault slip of 21.3 m and a fault width of 119.9 km. The moment magnitude of the source fault was calculated as 8.9, which is close to the fault parameters estimated using the geodetic and seismological methods. The proposed method is expected to contribute to the effective risk assessment of regional tsunami hazards from the geologic records of past tsunamis in various regions.

## **Chapter 4. Estimation of parameters of source fault model with heterogenous slip from tsunami deposits across diverse regions by DNN inverse model**

### **4.1 Introduction**

Accurate estimation of tsunami source fault model is essential for risk assessment of tsunamis. The historical and geological records implied that the Pacific coast of northeastern Japan suffered from large-scale tsunamis repeatedly. Among these tsunamis, some were estimated to have originated from Japan Trench repeatedly as subduction zone earthquakes (see Chapters 1 and 3 in detail). The entire behavior of tsunamis can be predicted using the 2D forward model calculation assuming the source fault model (e.g., Imamura et al., 2012). Thus, assessing the parameters for the source fault model of repeated large tsunamis will contribute to the disaster prevention planning for future events.

Numerous fault models have been proposed for the 2011 Tohoku-oki earthquake, and most of them implied the complexity of the source fault of this event. The existence of the large slip zone around the epicenter was inferred by several models, such as the model proposed based on GPS data before and after the earthquake (e.g., Ozawa et al., 2012). The fault model based on temporal change of the water level also implied the huge slip zone around the trench axis, which is responsible for the anomalous coastal tsunami height along the Sanriku coast (Satake et al., 2013). These results suggest that considering the source fault with heterogenous slip is necessary to estimate the tsunami behavior in detail.

In Chapter 3, the inverse model was developed to reconstruct the parameters of the single-segment fault model from the tsunami deposit distributed in the Sendai Plain.

Although this inverse model successfully estimated the source fault parameters and the magnitude of the earthquake solely from the tsunami deposit in a single region, it should be acknowledged that this approach comes with several constraints. Due to the limitation of using information from only a single region, the model had to rely on a priori assumption on the fault extent (i.e., 500 km) and the position. In addition, using a complex fault model where the slip displacement can be heterogeneous was impossible.

To address these limitations, a new inverse analysis method is proposed in this chapter to reconstruct the parameters of the complex source fault model from tsunami deposits in multiple different regions. The inverse model proposed is improved to estimate the heterogeneity of the slip distance in the fault plane in addition to the location of the source fault.

## **4.2 Method**

### **4.2.1 Source fault model**

The Headquarters for Earthquake Research Promotion (HERP) compiled fault parameters of various types of earthquakes and associated tsunamis to characterize source faults with simplified parameters (HERP, 2017). This method, called the tsunami recipe, parameterized the trench-axis fault along the Japan Trench that caused the 2011 Tohoku-oki tsunami. In this model, the fault is divided into three segments, which are the super large slip (SLS), large slip (LS), and background (BG) zones, as shown in Fig. 4-1.

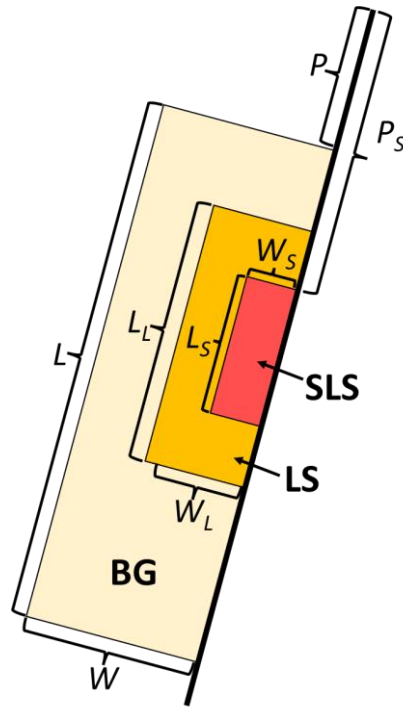


Fig. 4-1. Source fault model for this study based on tsunami recipe. Each segment is referred to as BG (Background), LS (Large Slip), and SLS (Super Large Slip).  $L$ ,  $L_L$  and  $L_S$  are the lengths of BG, LS, and SLS, respectively.  $W$ ,  $W_L$  and  $W_S$  are the widths of BG, LS, and SLS, respectively.  $P$  and  $P_S$  are the positions of the fault segments defined by the distance from the edge of the Japan trench to the Northeastern edge of BG and SLS.

The source fault model providing the spatial distribution of the initial sea-surface elevation to the forward model is defined by five primary parameters: the length  $L$  (km), width  $W$  (km), the position of the BG zone  $P$  (km), the position of the SLS zone  $P_S$  (km) and the average slip displacement  $D$  (m) of the fault. Here, the position of the fault was defined as the distance from the edge of the Japan Trench to the northeastern edge of the BG zone  $P$  (km) or the SLS zones, and the edge of the Japan Trench was defined as a junction point of the Japan and Kuril Trenches. The BG, LS, and SLS zones were supposed to be attached to the Japan Trench, and the long-axis direction of the fault was set parallel to the Trench. Other parameters of the fault, including the lengths  $L_L$  (km) and  $L_S$  (km), the widths  $W_L$  (km) and  $W_S$  (km) the slip displacements  $D_L$  (m) and  $D_S$  (m) of

the LS and SLS zones, as well as the position of the LS zone  $P_L$  (km), were determined by their empirical relationships with the primary parameters, whose procedures were described as follows (HERP, 2017).

The areas  $S_S$  (km<sup>2</sup>) and  $S_L$  (km<sup>2</sup>) and the slip displacement  $D_S$  (m) and  $D_L$  (m) of the SLS and LS zones were estimated by equations 4.1 to 4.4.

$$S_S = \xi_S \cdot S \quad (4.1)$$

$$S_L = \xi_L \cdot S \quad (4.2)$$

$$D_S = r_S \cdot D \quad (4.3)$$

$$D_L = r_L \cdot D \quad (4.4)$$

Based on the relation between the normalized slip ratio and the cumulative fault areas of the giant earthquakes, the empirical coefficients of these equations were set to  $\xi_S = 4$ ,  $\xi_L = 2$ ,  $r_S = 0.1$ ,  $r_L = 0.2$ . Then, assuming the geometric aspect ratio of SLS and LS zones are equal to the BG zone, the lengths  $L_S$  and  $L_L$  and the widths  $W_S$  and  $W_L$  were determined from the areas  $S_S$  and  $S_L$ .

The empirical relationship predicts the seismic moment  $M_0$  (Nm) from the fault area  $S$  (km<sup>2</sup>) and the average stress drop  $\Delta\sigma$  (MPa) as equation 4.5 (Eshelby, 1957).

$$M_0 = 16/(7\pi^{3/2}) \cdot \Delta\sigma \cdot S^{3/2} \quad (4.5)$$

In the cases of interplate earthquakes along the rims of the Pacific Plate around Japan,  $\Delta\sigma$  is estimated to be 4.3 (Fujiwara et al., 2015).

The following procedures estimate the seismic magnitude resulting from the fault described by the parameters above. The relationship between the average slip displacement  $D$  (m) and seismic magnitude  $M_0$  is expressed as the following equation 4.6:

$$D = M_0/(\mu \cdot S) \quad (4.6)$$

where  $\mu$  (N/m<sup>2</sup>) is the modulus of the rigidity of the fault. The standard values for the modulus of the rigidity were proposed by the Japan Society of Civil Engineers (2016),

which vary depending on the depths of entire fault planes. This study used the value of  $5.0 \times 10^{10}$  (N/m<sup>2</sup>), assuming that the fault plane is spread over above and below the 20 km depth. The relationship between moment ( $M_0$ ) and moment magnitude ( $M_w$ ) takes the form (HERP, 2017):

$$M_w = \frac{2}{3} \log M_0 + 6.07 \quad (4.7)$$

#### **4.2.2 Topographic settings and depositional features of the study areas**

This study analyzed the tsunami deposits distributed in the three regions of northeastern Japan: the Sendai Plain in the Miyagi Prefecture, the Odaka Area in the Fukushima Prefecture, and the Rikuzentakata in the Iwate Prefecture. We performed an inverse analysis of tsunami sediment data obtained from these areas.

The study area of the Sendai Plain located on the right bank of the Nanakita River in Sendai City, Miyagi Prefecture, Japan (Fig. 4-2), where the 2011 Tohoku-oki tsunami deposit was investigated three months after the event (Abe et al., 2012; Naruse and Abe, 2017). The area is characterized by flat and wide topography extending about 5 km inland from the shoreline.

Naruse and Abe (2017) measured the thickness and grain-size distribution of the tsunami deposit in Sendai Plain along the transect established perpendicular to the shoreline (Fig. 4-2). Along this transect, the tsunami inundated up to 4.02 km inland from the shoreline. The sandy tsunami deposit in this region was mainly composed of medium sands, and the thickness of the sandy tsunami deposit exhibited a landward thinning trend (Fig. 4-3).

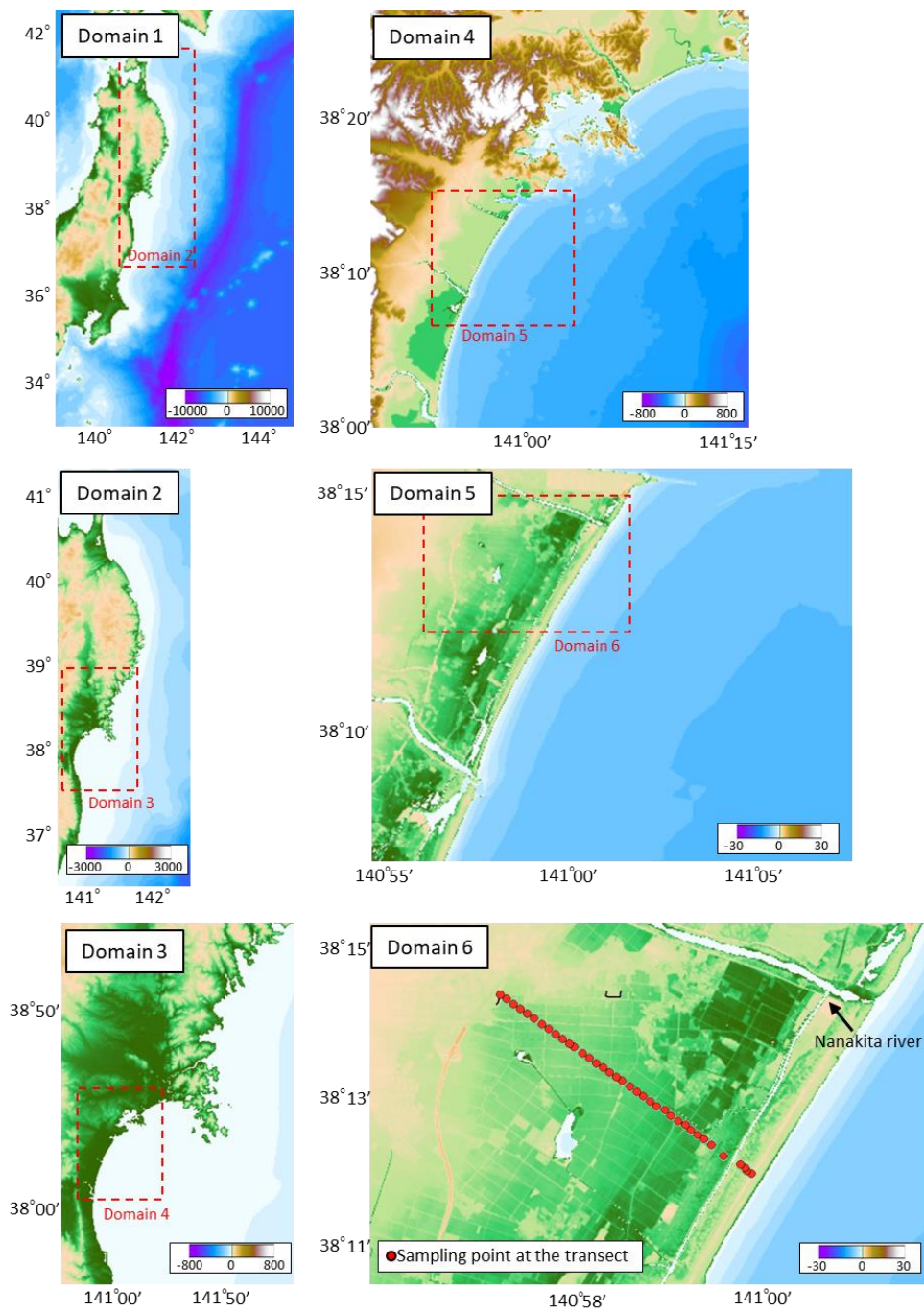


Fig. 4-2. Location of study area for Sendai is shown with bathymetry data and domains used for forward model. Red dashed box of each domain indicates the smaller domain in nesting grid system. Domain 6 covers Sendai, and transect used for the output of the forward model is shown.

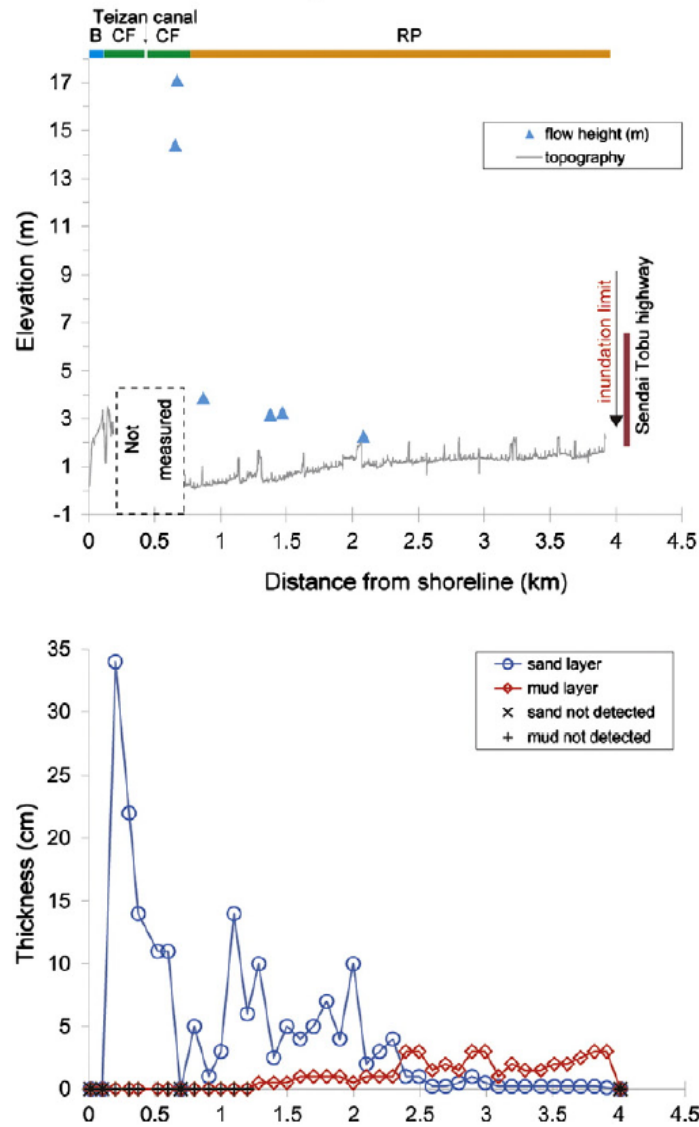


Fig. 4-3. Flow height and thickness of tsunami deposit observed at the transect (Fig. 4-2) at Sendai Plain (Abe et al., 2012).

The second study area is the Odaka region, Minami-soma City, Fukushima Prefecture, approximately 150 km west of the epicenter of the 2011 earthquake and 80 km south of Sendai City (Fig. 4-4). Iijima et al. (2021) conducted the field survey in June and July 2013. Although the survey was conducted about two years after the 2011 Tohoku-oki tsunami, reconstruction work, such as soil modification of paddy field or raising work of lowland area, was highly limited because the area is 10 km north of

Fukushima Daiichi Nuclear Power Station and entry to this area was strictly limited. In addition, there was no severe rain or flooding after the 2011 Tohoku-oki tsunami, which means that tsunami deposits in this area could be well preserved until the field survey. The area is relatively flat, less than 2 m above the mean sea level in elevation.

A 2.6 km long transect was established from the shoreline to the inundation limit, and thickness and grain-size distribution of the tsunami deposit was measured at 50 m intervals along the transect (Fig. 4-4). Along this transect, the tsunami inundated up to 2.6 km inland from the shoreline. In this area, the source, thickness, and sedimentary structure of tsunami deposits are inferred to have been affected by artificial structures. Sandy tsunami deposits were estimated to have originated mainly from the backshore, which was deeply eroded at the landward side of the dike due to tsunami overflow. The thickness of the tsunami deposit was affected by three paddy roads that exist perpendicular to the transect (Roads 1–3 in Fig. 4-5). The thickness of tsunami deposits was maximum at 50 to 100 m seaward of the paddy road and then suddenly decreased at the landward region of the road.

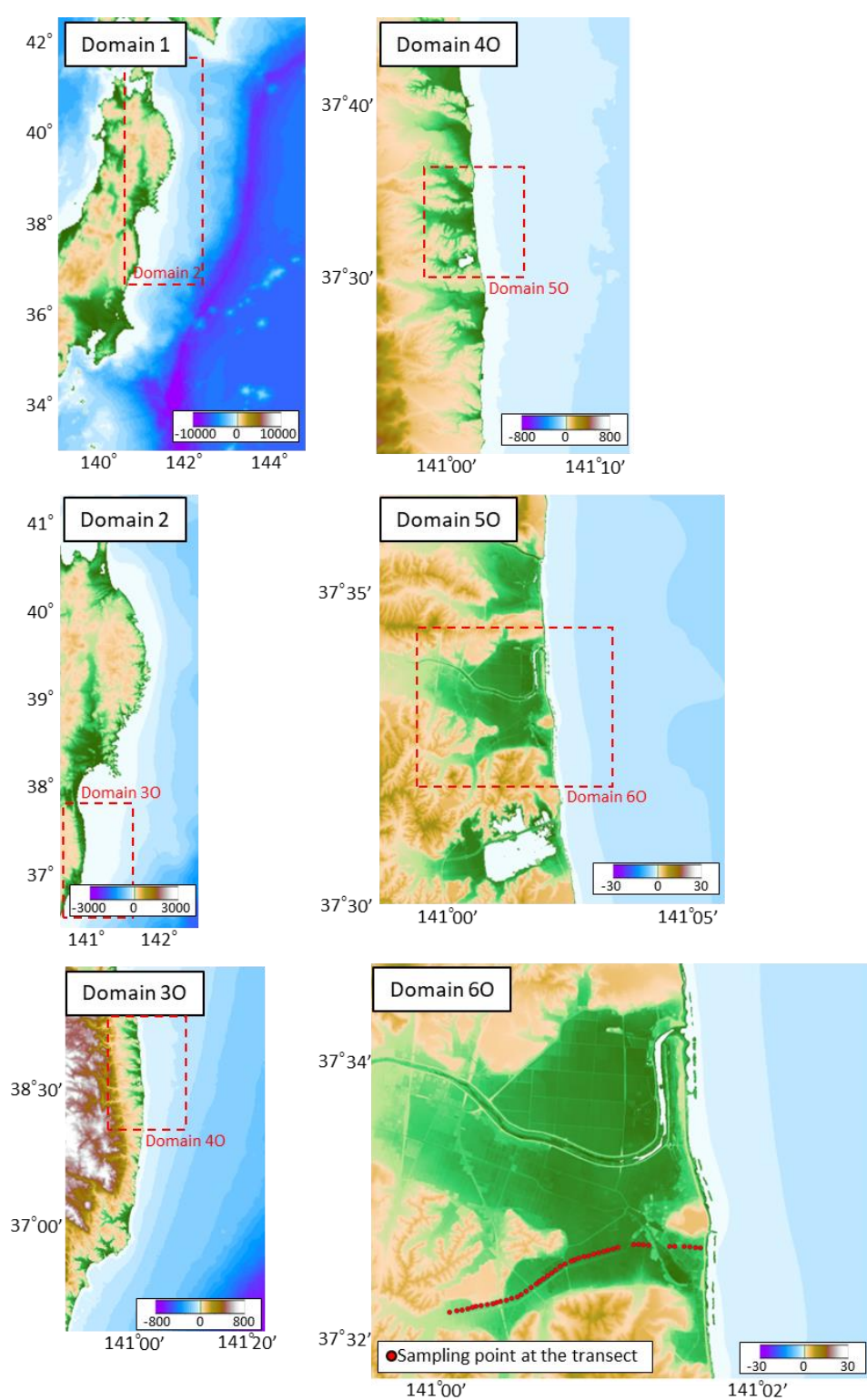


Fig. 4-4. Location of study area for Odaka is shown with bathymetry data and domains used for forward model. Red dashed box of each domain indicates the smaller domain in nesting grid system. Domain 6 covers Odaka, and transect used for the output of the forward model is shown.

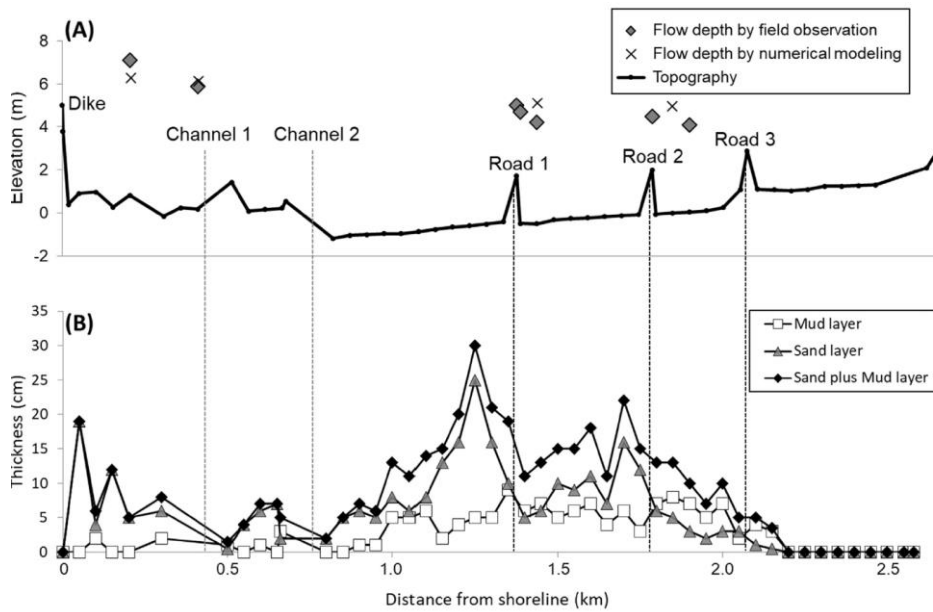


Fig. 4-5. (A) Topography and flow depth of tsunami. (B) Thickness of sandy and muddy tsunami deposits along the transect (Iijima et al., 2021).

The third study area is Rikuzentakata City, Iwate Prefecture, which is approximately 130 km west of the epicenter of the 2011 earthquake and 100 km northeast of Sendai City. The area is part of the Ria coast, which is characterized by narrow valleys between mountains along the shoreline (Fig. 4-6).

Naruse et al. (2012) conducted a field survey of this area in April and June 2011. They surveyed the thickness, grain size distribution, and sedimentary structures of the tsunami deposits at the pits dug to cover a large part of the inundated area. In this area, tsunami deposits were distributed across the entire inundated area. The transported sediment started to settle down about 500 m from the shoreline, and the maximum thickness (31.5 cm) was observed about 600 m from the shoreline. Then, the thickness decreased landward, although local variations were observed concerning topographic depressions (Fig. 4-7).

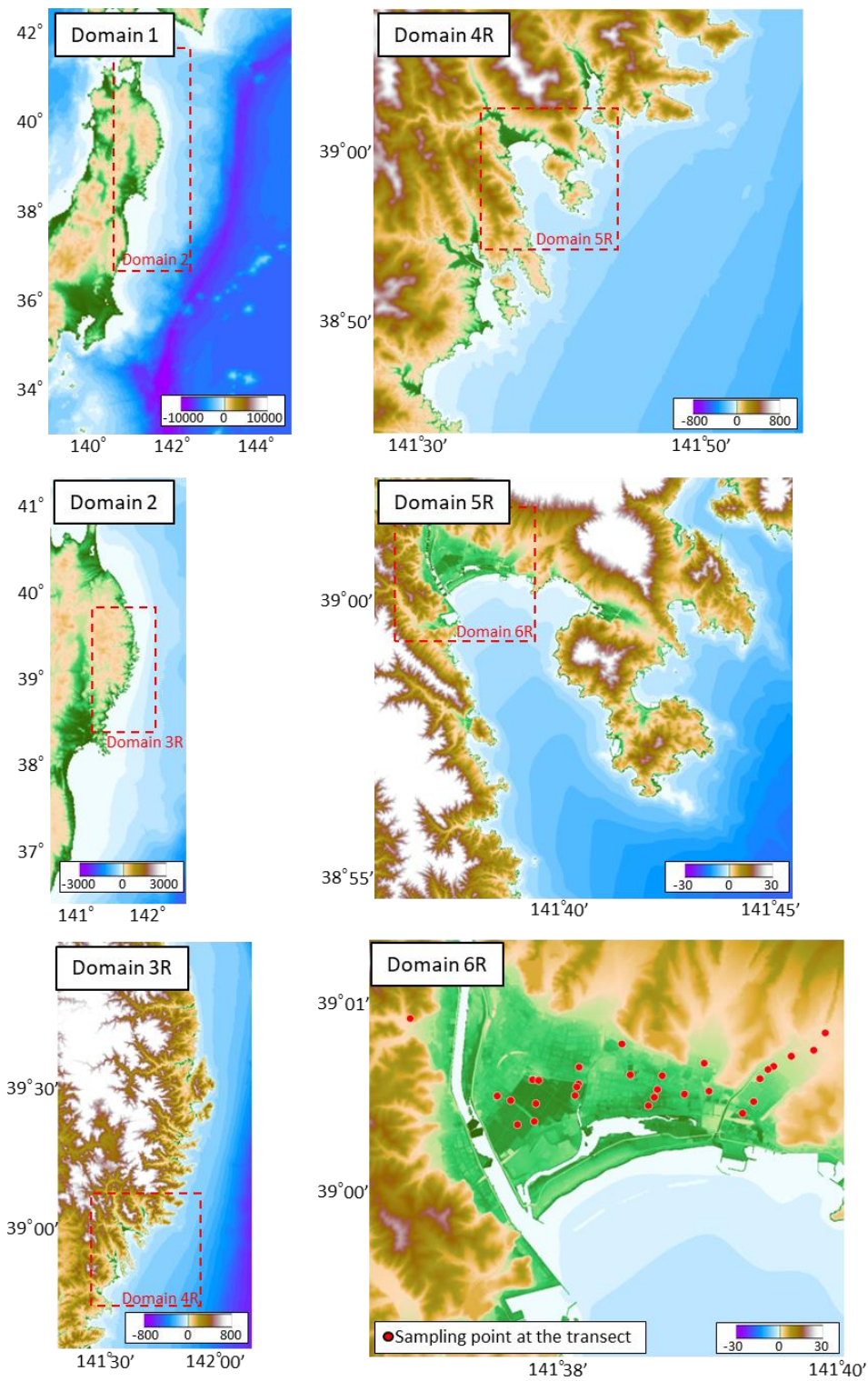


Fig. 4-6. Location of study area for Rikuzentakata is shown with bathymetry data and domains used for forward model. Red dashed box of each domain indicates the smaller domain in nesting grid system. Domain 6 covers Rikuzentakata, and transect used for the output of the forward model is shown.

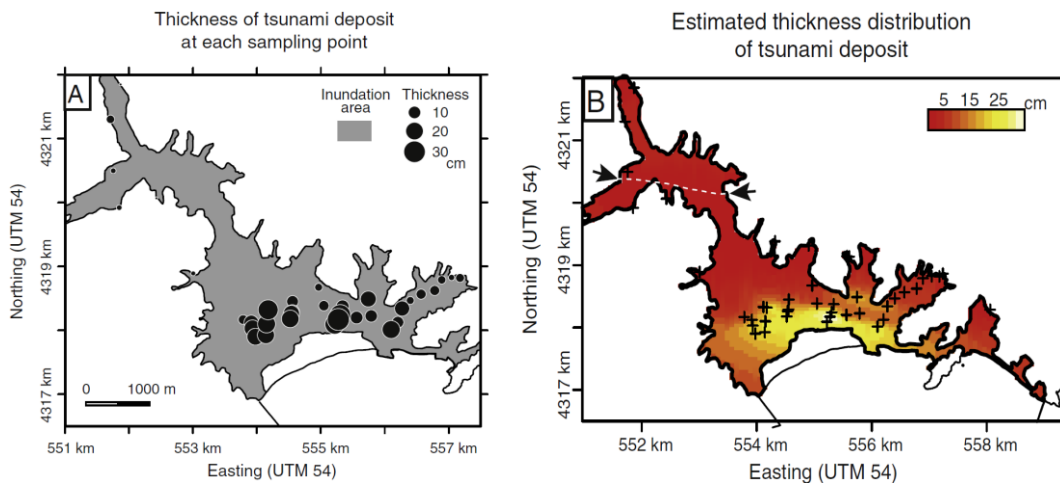


Fig. 4-7. Thickness of tsunami deposit (Naruse et al., 2012)

#### 4.2.3 Forward model calculation for producing training and test datasets

Delft3D-FLOW was chosen as the forward model of this study, which has been used for the simulation of tsunamis and transportation of sediments by tsunamis (e.g., Apotsos et al., 2011a, 2011b; Watanabe et al., 2018). See Chapter 2 for the details of this numerical model.

The arrangement of the computational domains for the forward model targeting Sendai followed the scheme of Watanabe et al. (2018), which is composed of the six nested calculation domains. Spatial grid sizes for the Domains 1–5 were 3645 m, 1215 m, 405 m, 135 m, 45 m, respectively. The Domain 6 was 15 m in the spatial grid size. The computational domains for the forward model targeting Odaka and Rikuzentakata are also composed of six nested domains for each region. The Domains 1–2 were the same as Sendai, while the Domains 3O–6O for Odaka and the Domains 3R–6R for Rikuzentakata were prepared separately. The Domains 6O and 6R were 15 m in the spatial grid size. The time step length was 0.3 seconds in all domains. Domain 1 covered the most extensive region among all domains, which contained Japan Trench and the entire region of

northeast Japan. The domains covered progressively smaller areas as spatial resolution increased. Domains 6, 6O, and 6R, which had the grids of the highest spatial resolution, covered the Sendai, Odaka, and Rikuzentakata regions, respectively. Sediment transport and depositional processes were calculated only in these Domains 6, 6O, and 6R.

In this study, the topographic datasets were based on a 5-m-mesh digital elevation model (DEM) provided by the Geospatial Information Authority of Japan that was constructed before the 2011 Tohoku-oki earthquake. The source areas of the tsunami deposits were set to be the region over the seabed, beach, and aeolian dunes in each study region, following the estimation by Sugawara et al. (2014), Iijima et al. (2021), and Naruse et al. (2012). The grain size distribution of the surface sediment in the source area was discretized into four-grain size classes (0.14, 0.25, 0.42, and 1.00 mm). We assumed that grain size distribution was spatially uniform in the source area, whereas a fraction of each grain size class was subject to be estimated by the inverse analysis.

In total, 728 sets of the parameters of the source fault model and tsunami deposit data were generated as the training, validation, and test datasets for the DNN inverse model. The source fault parameters were randomly generated to produce the training datasets. The fault length  $L$  and width  $W$  were generated randomly from 50 to 500 km and 25 to 250 km, respectively. The source fault position  $P$  was generated randomly from 0 to 500 km. The position of SLS  $P_S$  was also generated randomly based on equation 4.8 so that the position of the SLS zone did not extend beyond the BG zone.

$$(L|L - L_S)/2 < P_S < L - L_S L (L_L - L_S)/2 \quad (4.8)$$

The range for generating the average slip  $D$  was from 3 to 13 m. Other fault model parameters were obtained according to the abovementioned parameters following the procedures described in the previous section. The moment magnitudes of the resultant

fault models were distributed from Mw 7.9 to 9.2 (Fig. 4-8).

One random number for each grain size class was generated within the same range independently for each region. Then, the fraction of bottom sediment in the source area for each grain size class was set as a value normalized by the sum of those random numbers.

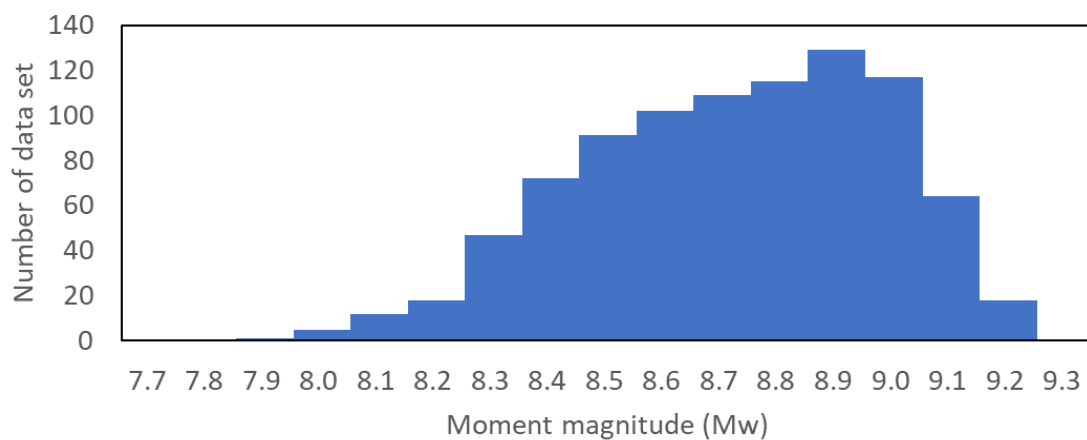


Fig. 4-8. Histogram showing moment magnitude of initial fault parameter generated as training data for the inverse model.

#### 4.2.4 Training of inverse model using deep neural network

The DNN inverse model developed (Mitra et al., 2020) accepts the values of volume-per-unit areas of four-grain size classes at 111 sampling points (35 at Sendai, 45 at Odaka, and 31 at Rikuzentakata) at an input layer of the neural network, so that the input layer was composed of 444 nodes in total. The output layer was composed of 16 nodes that provided the estimates of initial fault and sediment parameters (fault width, length, position of BG, and position of SLS) in addition to fractions of four-grain size classes of source sediment for each region.

The inverse model was trained using an artificial dataset obtained by the iteration of the forward model calculation. The output of the inverse model was evaluated using

the loss function defined in equation 4.9 (Mitra et al., 2020):

$$J = \frac{1}{N} \sum (I_k^{f^m} - I_k^{NN})^2 \quad (4.9)$$

where  $I_k^{f^m}$  denotes the ground-truth parameters used to produce the  $k$ th training data and  $I_k^{NN}$  is the predicted parameters by the DNN. More details on the DNN training settings are given in Chapter 2.

## **4.3 Result**

### **4.3.1 Training of inverse model and validation with synthetic data**

The training with the artificial dataset successfully generated an inverse model of tsunami deposits without overlearning. In this study, the model was trained on 582 sets of training data, and 146 datasets were used to validate whether overlearning occurred in the training process. The learning curve of the model (Fig. 4-9) indicated that both training loss and validation loss rapidly decreased and converged to the nearly constant value, which implies that no overlearning occurred through the training process.

The test results with 35 sets of artificial data proved the performance of the inverse model. The values predicted by the inverse model agree well with the values given to the original forward model so that the plots converged along the 45-degree line (Figs. 4-10–13). Among the fault parameters, however, the position of the BG zone does not indicate a clear fitting between the original and estimated values compared with the test results of other parameters. The predicted values of the moment magnitude of the fault model (equation 4.7) also matched with the original values (Fig. 4-14).

The relationship between the loss function and the number of training datasets (Fig. 4-15) indicated that the result of the model training improved as the number of training datasets increased, while the value of the loss function converged to the constant value when the number of the training data set reached more than 500.

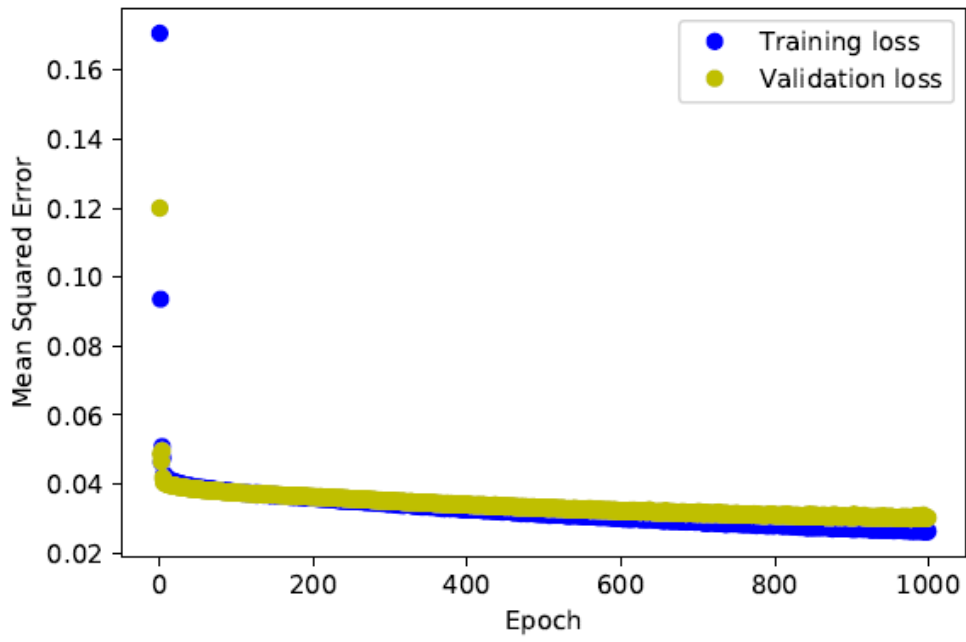


Fig. 4-9. Learning history of the inverse model with artificial data sets.

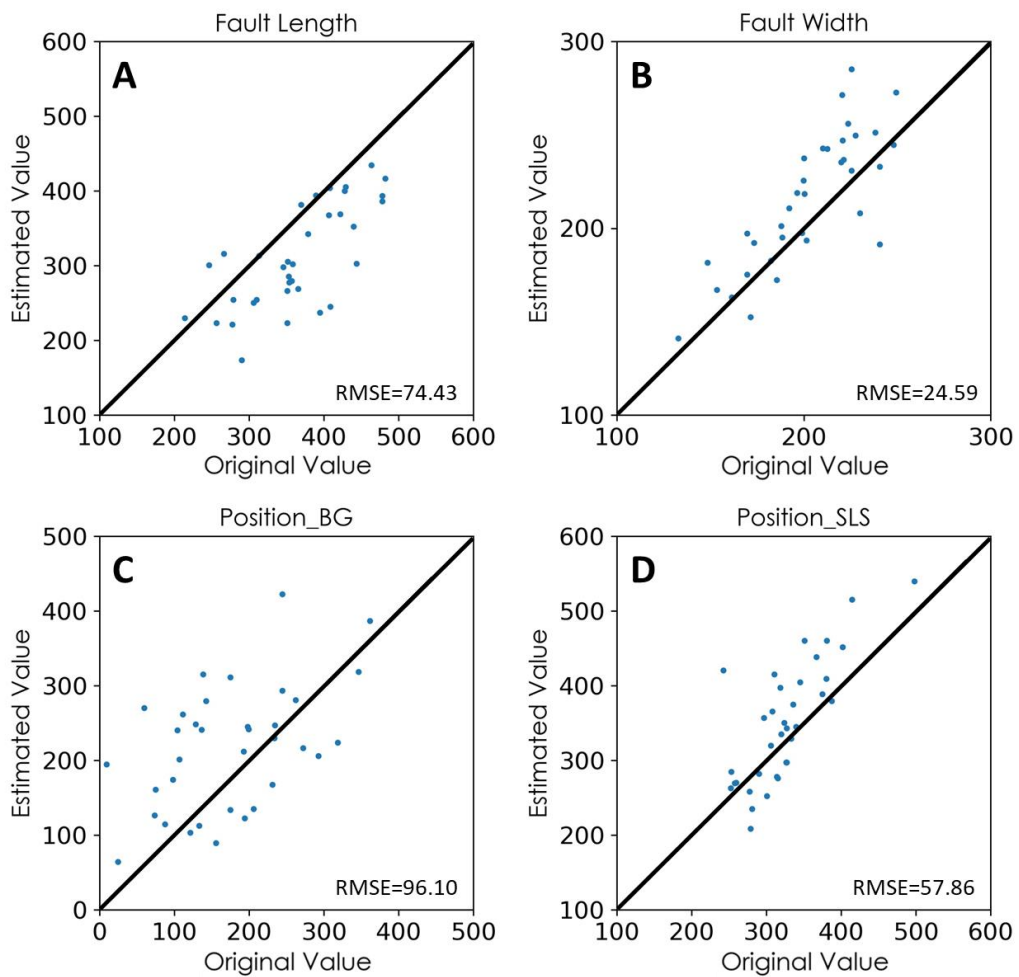


Fig. 4-10. Result of test for (A) fault length, (B) fault width, (C) position of BG, and (D) position of SLS. The plot with predicted value of the inverse model against the original values were distributed along the 45-degree line, which indicate that input and estimated value for inverse model well correspond each other.

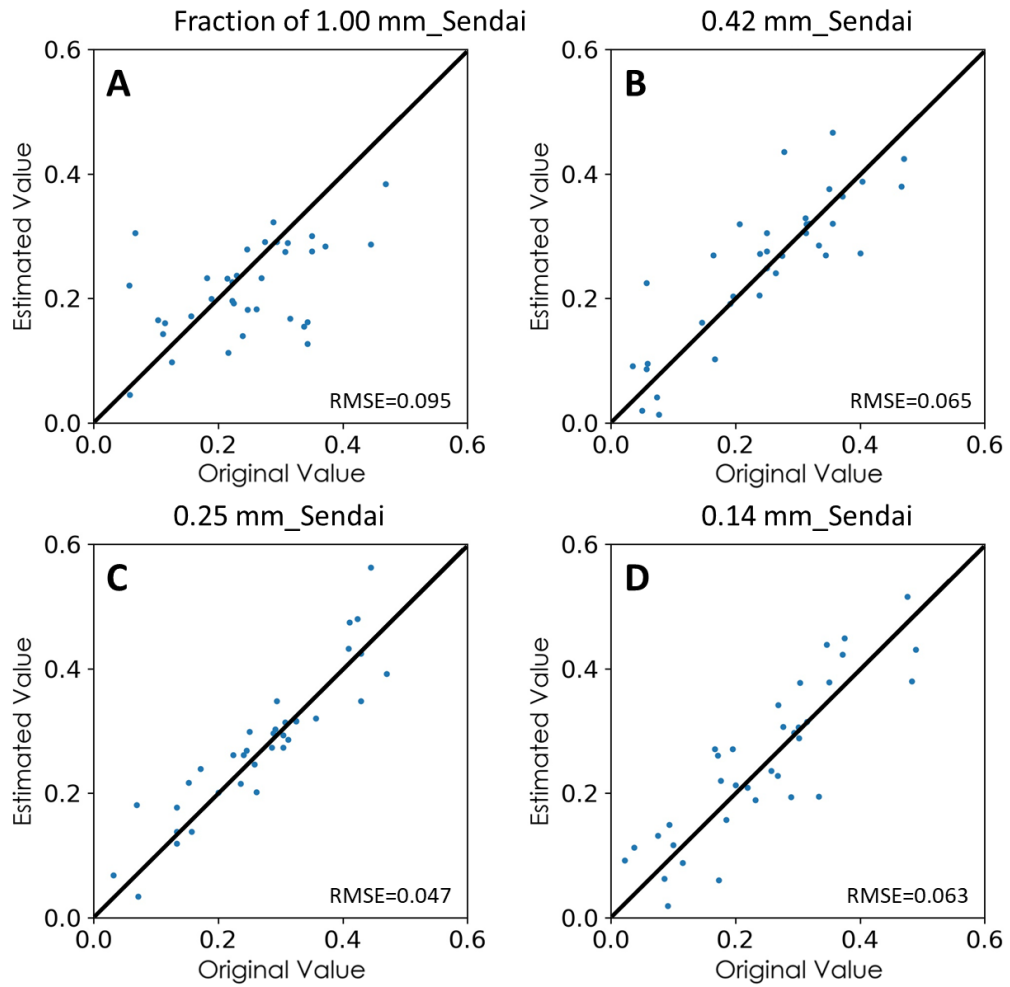


Fig. 4-11. Result of test with synthetic data set for four grain size classes (A: 1.00 mm, B: 0.42 mm, C: 0.25 mm, D: 0.14 mm) for Sendai.

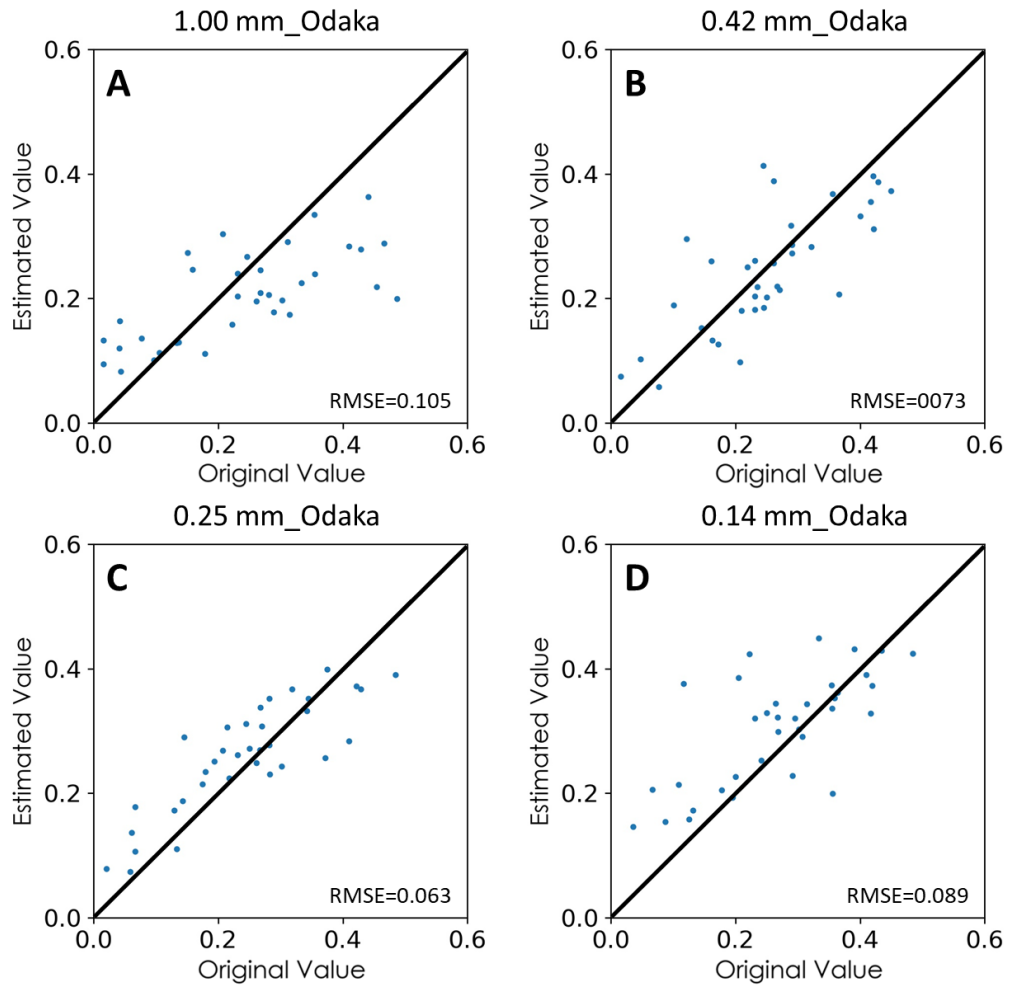


Fig. 4-12. Result of test with synthetic data set for four grain size classes (A: 1.00 mm, B: 0.42 mm, C: 0.25 mm, D: 0.14 mm) for Odaka.

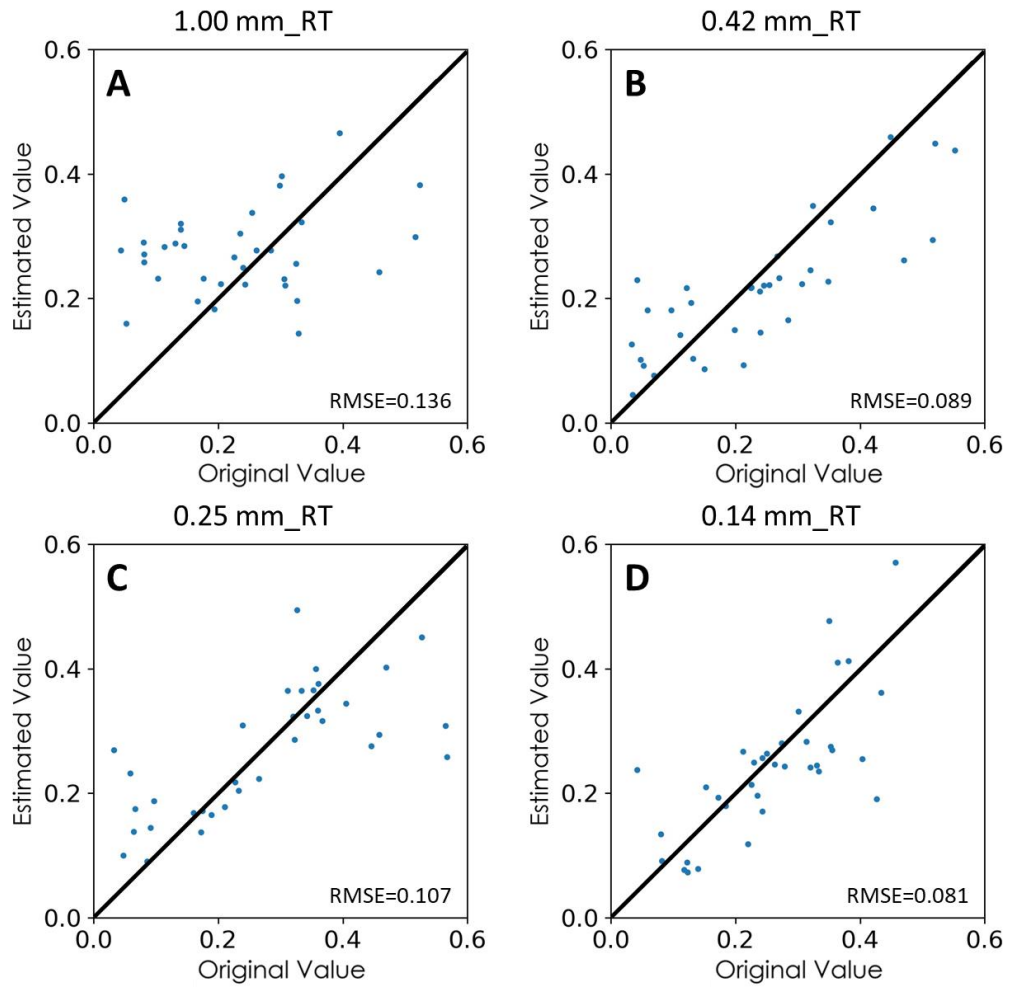


Fig. 4-13. Result of test with synthetic data set for four grain size classes (A: 1.00 mm, B: 0.42 mm, C: 0.25 mm, D: 0.14 mm) for Rikuzentakata (RT).

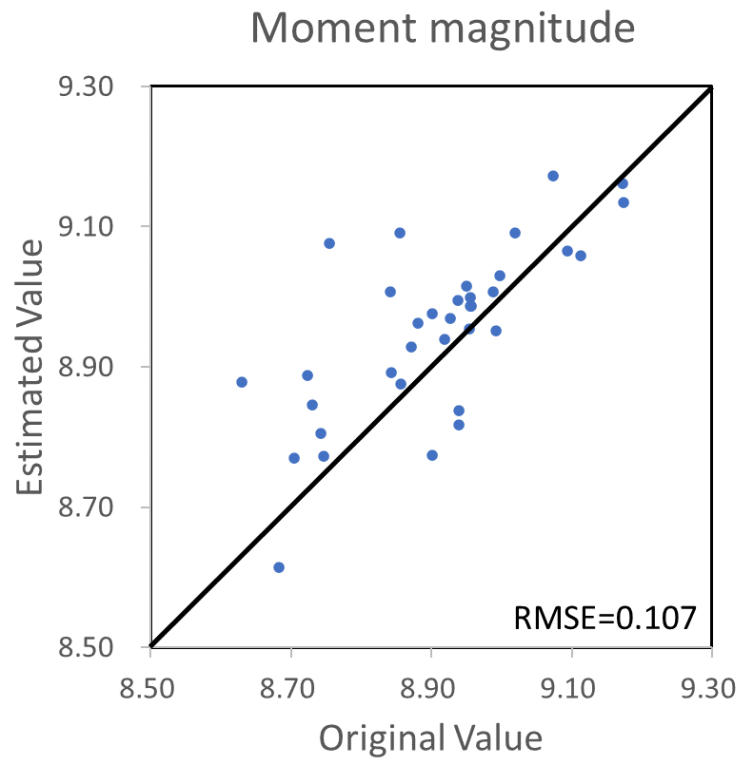


Fig. 4-14. Result of test with synthetic data set for moment magnitude calculated from fault width and slip.

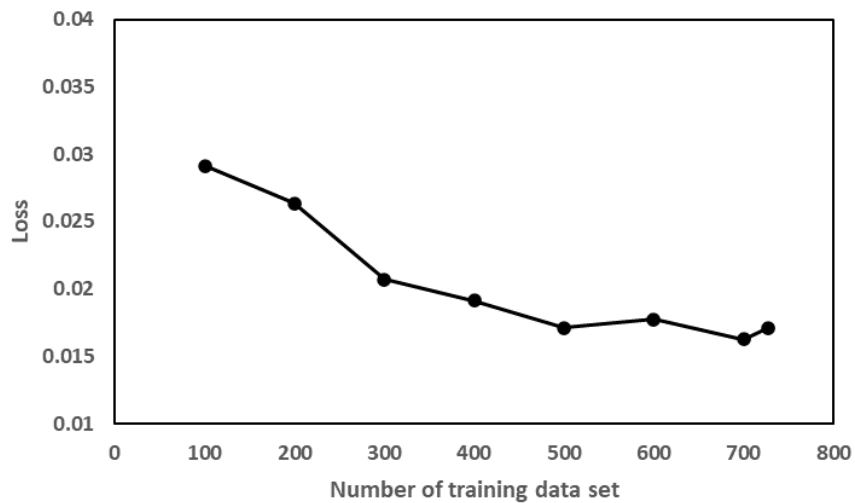


Fig. 4-15. Relationship between number of training data sets and loss function.

### **4.3.2 Inverse analysis of the 2011 Tohoku-oki tsunami**

The DNN inverse model was applied to the tsunami deposit formed by the 2011 Tohoku-oki tsunami. The model predicted the length and width of the source fault of this event as 464.5 km and 162.0 km, respectively (Table 4-1). The positions of BG and SLS were estimated to be 196.9 km and 380.9 km from the edge of the Japan Trench. Other fault parameters were calculated according to the predicted values of the BG zone described above (Table 4-2). For Sendai Plain, estimated fractions of grain-size classes of basal sediment in the source area were 12.0 %, 17.7 %, 60.5 %, and 10.7 %, respectively. For Odaka, fractions of grain-size classes were 24.7 %, 11.6 %, 47.2 %, and 17.3 %, respectively. For Rikuzentakata, fractions of grain-size classes were 12.3 %, 35.0 %, 39.7 %, and 13.5 %, respectively.

To examine the validity of the inversion result, the forward model calculation was performed using these estimated source fault parameters to obtain the thickness and grain size distributions of the tsunami deposits in the study areas. The resultant thickness and grain size distribution of the sandy tsunami deposits on the Sendai Plain, Odaka, and Rikuzentakata regions (Figs. 4-16–18) exhibited the landward fining trend and correlated well with the measured values. The exceptions are the deviation between predicted values in the region more than 2500 m landward from the shoreline in the Sendai Plain and the distribution of the grain size class 0.42 mm in the Odaka region.

Table 4-1. Estimated fault parameters and initial percentage of sediment from inverse analysis.

Parameter	Predicted results
Fault length (km)	464.5
Fault width (km)	162.0
BG position (km)	196.9
SLS position (km)	380.9
1.00 mm_Sendai (%)	12.0
0.42 mm_Sendai (%)	17.7
0.25 mm_Sendai (%)	60.5
0.14 mm_Sendai (%)	10.7
1.00 mm_Odaka (%)	24.7
0.42 mm_Odaka (%)	11.6
0.25 mm_Odaka (%)	47.2
0.14 mm_Odaka (%)	17.3
1.00 mm_RT (%)	12.3
0.42 mm_RT (%)	35.0
0.25 mm_RT (%)	39.7
0.14 mm_RT (%)	13.5

Table 4-2. Estimated fault parameter for each segment.

Parameter	Predicted results
Fault length (km)	464.5
Fault width (km)	162.0
BG slip (m)	3.3
LS length (km)	338.2
LS width (km)	93.1
LS slip (m)	19.7
SLS length (km)	195.3
SLS width (km)	53.7
SLS slip (m)	39.4

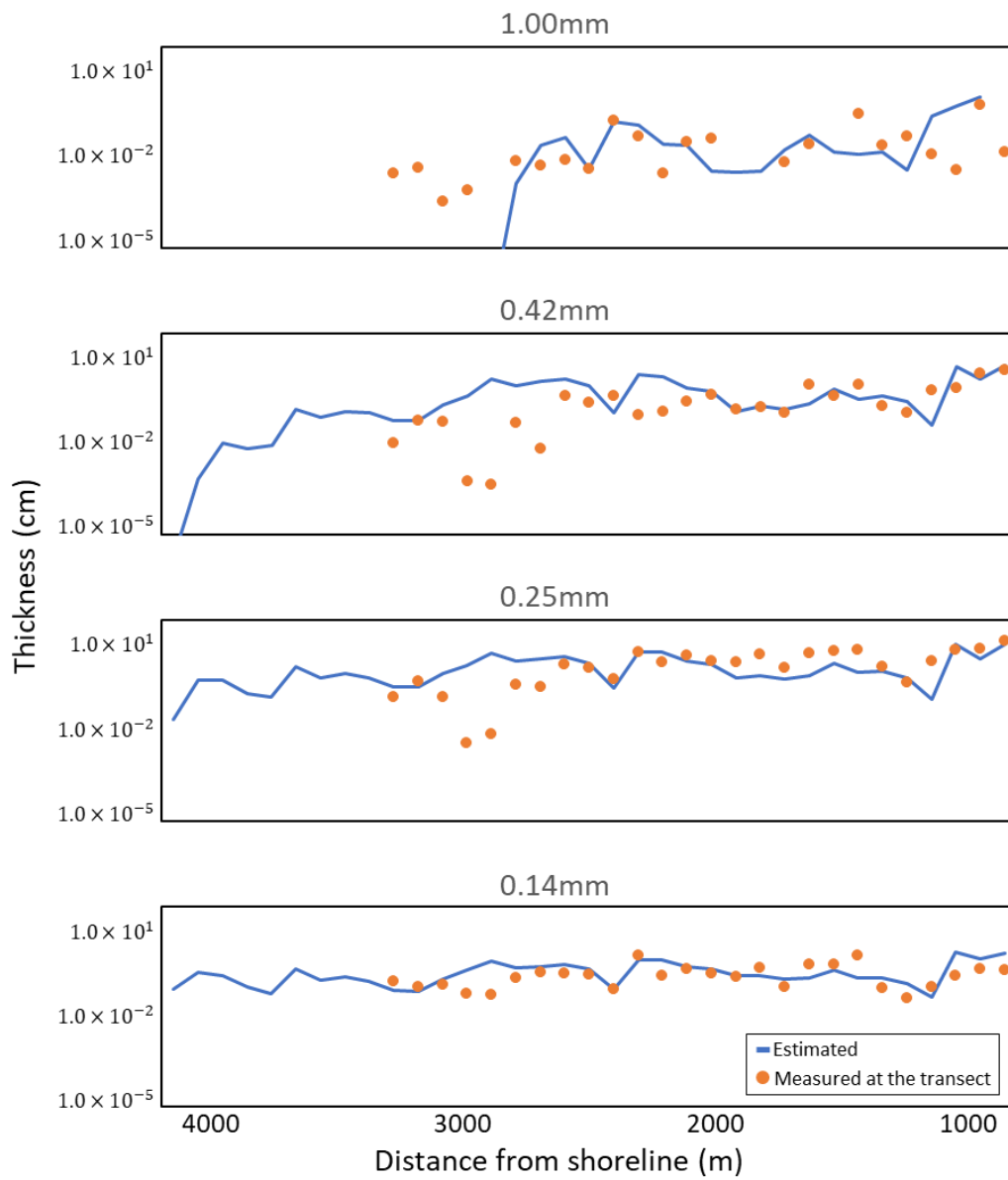


Fig. 4-16. Comparison of measured and estimated thickness of sandy tsunami deposit along the transect at Sendai.

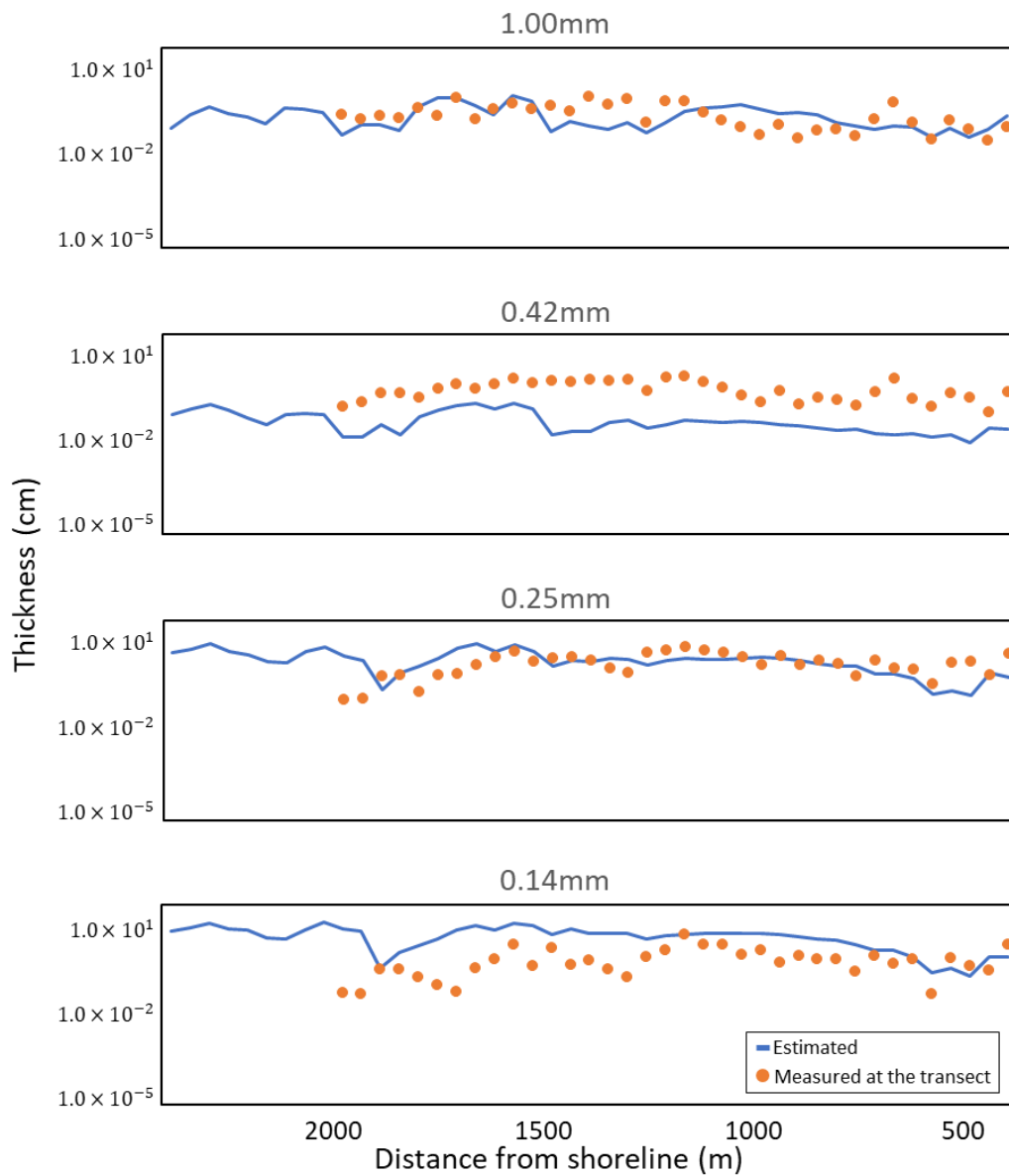


Fig. 4-17. Comparison of measured and estimated thickness of sandy tsunami deposit along the transect at Odaka.

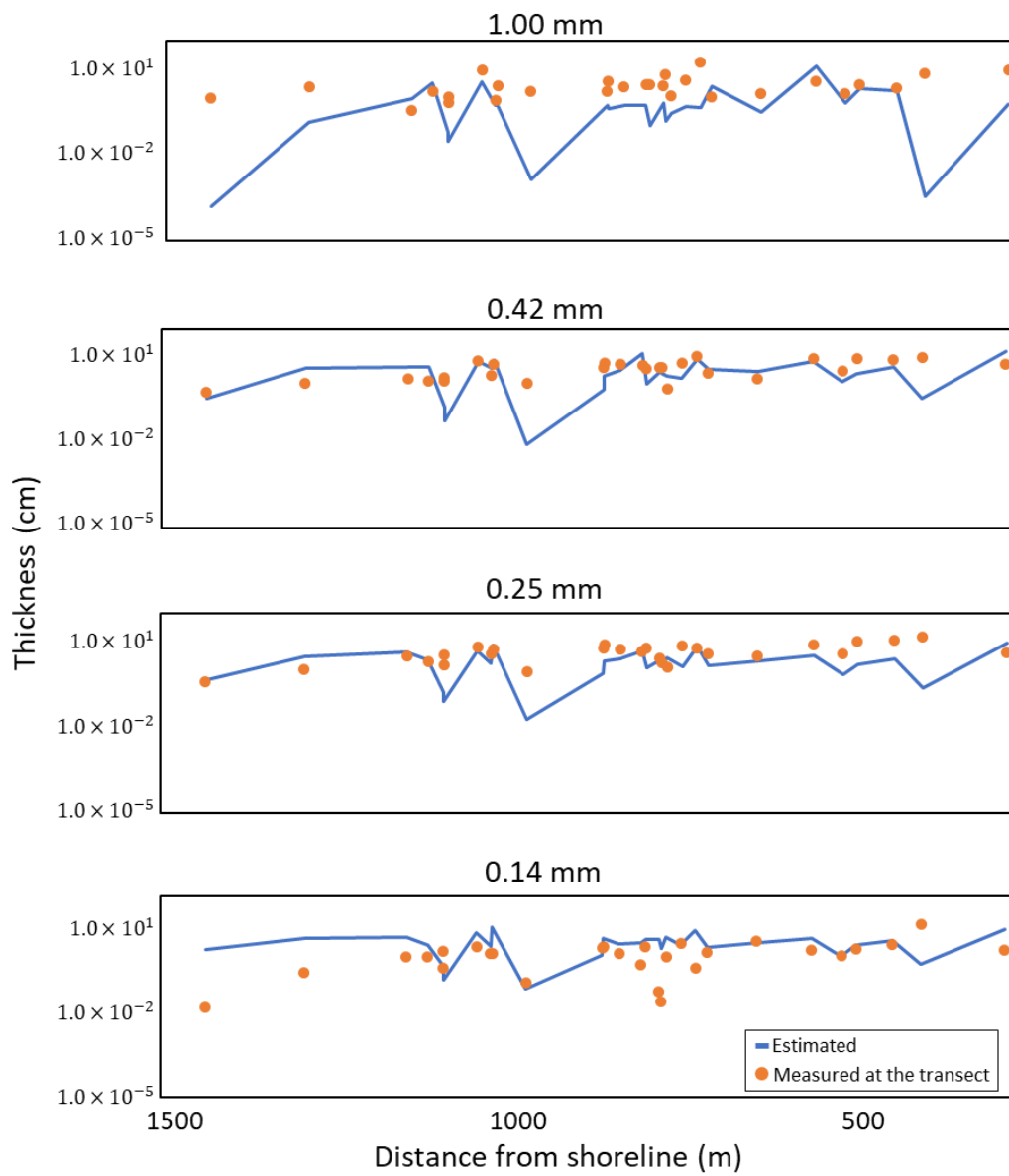


Fig. 4-18. Comparison of measured and estimated thickness of sandy tsunami deposit at Rikuzentakata.

## **4.4 Discussion**

### **4.4.1 Comparison with fault parameters determined by existing studies**

The inverse model proposed in this study predicted source fault parameters as shown in Table 4-1. According to a compilation study on the estimated fault parameters of the 2011 Tohoku-oki tsunami (Lay, 2018), the distribution of the fault slip displacement is quite diverse from study to study, and there is no definitive common consensus for the reconstruction result of the fault extent and slip displacement. Nevertheless, the estimated coseismic slip ranges from 10 to 30 m around the trench axis, then decreases to 0 to 15 m at around 100 km from the trench axis. These estimates are consistent with the inversion results of our model (Fig. 4-19).

Based on the estimated area of the source fault and the relationship between area and magnitude (equation 4.8), the moment magnitude is calculated as 9.0. A review of the fault model for the 2011 Tohoku-oki earthquake summarized that the moment magnitude of this event is estimated to be 9.0–9.1 in most studies (Lay, 2018). The estimated moment magnitude from the tsunami deposit in this study was 9.0, comparable to this value. A slight underestimate may derive from a lack of information on the tsunami deposit near the north or south edge of the source fault.

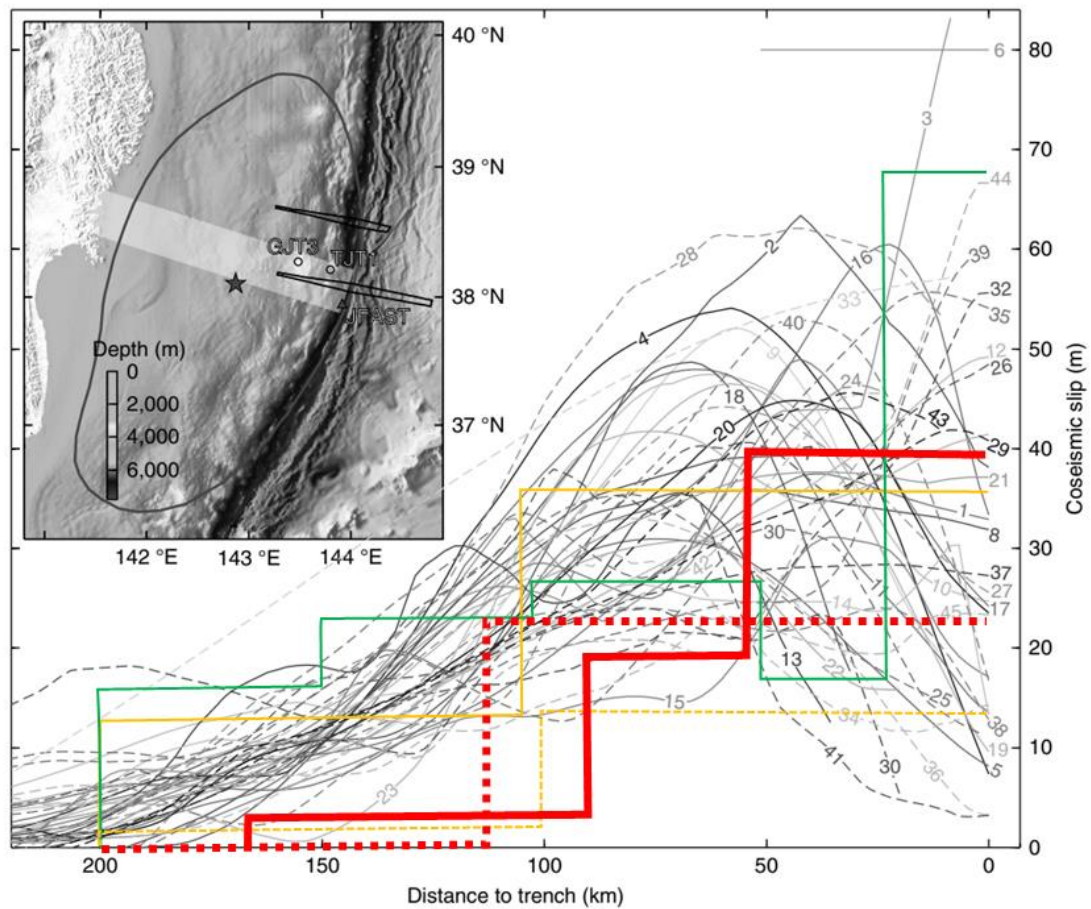


Fig. 4-19. Comparison of previous fault model with this study. Coseismic slip against distance to the trench is shown in the result of a compilation study by Lay (2018). The number of each line is identified in Lay (2018). The red solid line indicates the fault model estimated from this study, and the red dotted line indicates that of Chapter 2. Green line is from Satake et al. (2013). The orange solid line is from Imamura et al. (2012). The orange dashed line is the averaged fault model of Imamura et al. (2012) by averaging the slip of each segment in a north-south direction.

#### 4.4.2 Advantages and limitations of the model

In this study, we improved the inverse method presented in Chapter 3 to estimate the fault model parameters with the heterogeneous slip from tsunami deposits observed in multiple locations. This model was enhanced from the previous inverse model (1) to estimate the location of the source fault and (2) to estimate the magnitude of the source fault model with multiple segments.

The great advantage of the model is its applicability to paleo-tsunami deposits, such as the 869 Jogan tsunami. The previous study estimated the source fault parameters from the tsunami deposits by assuming the location of the source fault (e.g., Sugawara 2011; Namegaya and Satake, 2014). This model only assumed that the source fault was a trench axis earthquake that occurred along the Japan Trench, and the location of the source fault was estimated through the inversion. Compared to other inverse models, the model developed in this chapter requires very few assumptions about source faults and is, therefore, suitable for paleo-tsunami deposits in geologic records where the wave source is unknown. Although reconstruction of paleo-topography is required to conduct the forward model calculation of the tsunami propagation and sediment transportation, applying the inverse model to paleo-tsunami deposits will contribute to a more accurate estimation of source fault for paleo-tsunami.

On the other hand, the precision of the estimated values by this inverse model was less than that of the model presented in Chapter 3. The reason may be because the number of training datasets was insufficient to estimate the target parameters, which doubles from that in Chapter 3. In addition, although we assumed only trench earthquakes as the wave source faults, tsunamis can also be generated by intra-plate earthquakes and outer-rise earthquakes in this area. In future studies, these types of fault parameters should also be considered as the initial parameters of the forward model.

## **4.5 Conclusions**

This study improved the inverse model to estimate the source fault parameter of the tsunami directly from tsunami deposits observed at multiple locations. The model utilized the DNN, which is trained by artificial datasets produced by the forward model of tsunami

propagation and sediment transportation at three regions: Sendai, Odaka, and Rikuzentakata. The inverse model was validated with synthetic datasets, and the model successfully reconstructed initial fault parameters, including length, width, and position. Then, we performed an inverse analysis of actual data from the 2011 Tohoku-oki tsunami deposit to test the applicability of the inverse model in natural cases. Our result demonstrated that the model was able to reconstruct fault parameters adequately, which were close to the fault parameters measured by other methods. Moment magnitude is estimated to be 9.0, which is also conformable to the previous study. Our method contributes to the risk assessment of the regional tsunami hazards by estimating the magnitudes of past tsunamis from geologic records in various regions.

## **Chapter 5. Conclusions**

### **5.1 Chapter summaries**

This study proposed a new inverse model of tsunami deposits using a DNN that enables the estimation of source fault parameters solely from tsunami deposits.

In Chapter 2, the equations constituting the forward model and the structures of the inverse model were described. Regarding the forward model, Delft3D-FLOW, which solves the nonlinear shallow water equations on a horizontal two-dimensional staggered grid, was selected for this study. The sediment transport is calculated by the transport equations for the suspended load and bedload. The inverse model used in this study is composed of DNN with three hidden layers. The forward model calculation was repeated with random initial fault conditions (fault slip and width) and the sediment grain size distribution in the source area to produce an artificial training data set. Then, DNN was trained to establish an inverse model. Compared to existing tsunami sediment inversion models, this study is a significant advance in that it directly estimates the parameters of the tsunami wave source fault and employs a 2D model in the forward model.

In Chapter 3, a new inverse model to estimate the fault model with homogeneous slip was proposed. The tests with the synthetic data set indicated that the inverse model can accurately estimate the fault parameters and the sediment grain size distribution. The inverse model was applied to the tsunami deposit formed by the 2011 Tohoku-oki tsunami. The model predicted 21.3 m in fault displacement and 119.9 km in fault width, close to the fault parameters measured by other methods. It is concluded that the new inverse model was successfully developed, and it is confirmed that the model can estimate reasonable fault parameters solely from tsunami deposits.

In Chapter 4, the model was improved to estimate the width, length, and location

of the source fault model with the heterogeneous slip from tsunami deposits observed at multiple locations. The fault model utilized the empirical relationships of the slip heterogeneity. The model was validated with synthetic datasets again, and then we performed an inverse analysis of the 2011 Tohoku-oki tsunami deposit observed in three regions: Sendai, Odaka, and Rikuzentakata. The model predicted 464.5 km in fault length and 162.0 km in fault width, and the northeast edge of the fault to be 196.9 km from the edge of the Japan Trench. This improved inverse model successfully reconstructed fault parameters, including lengths, widths, and locations of the source fault, which the previous model could not estimate (Chapter 3). The moment magnitude of the source fault is estimated to be 9.0 solely from the tsunami deposit, which is comparable to the previous studies ( $M_w = 9.0\text{--}9.1$ ). This is the first estimation of the moment magnitude of the earthquake from the inverse models of tsunami deposits.

## **5.2 Future research directions**

Although the model in Chapter 4 can estimate the parameters of the source fault with the heterogeneous slip, the tests with a synthetic data set implied less accurate estimation compared to the simple model shown in Chapter 3. Suppose this lesser performance of the inverse model can be attributed to insufficient training datasets; the model performance can be easily improved by increasing training datasets using the forward model. However, if the ability of the model to estimate complex fault parameters requires an increase in the number of study areas, it is not always possible to improve the prediction precision of the inverse model. When analyzing paleo-tsunami deposits, the number of areas where deposits are found cannot be increased as much as desired. In this sense, the inverse model for homogeneous slip faults in Chapter 3 can complement the inverse model for heterogeneous slip faults in Chapter 4. That is, when the amount of

information obtained from the survey is not enough, a simplified fault model can be used, whereas when the amount of information is large, an attempt can be made to reconstruct more complex information about earthquakes.

The model can be applied to paleo-tsunami deposits to estimate the magnitude of past earthquakes quantitatively. The 869 Jogan tsunami is the best candidate for this study because the Jogan tsunami deposit has been relatively well surveyed along the shoreline of NE Japan. Application of the model may contribute to estimating the source fault parameters of the Jogan tsunami, which helps verify the hypothesis that the 2011 Tohoku-oki tsunami is the recurrence of the Jogan tsunami.

The other direction of this study is to include other types of earthquakes for the subjects of inversion, such as outer rise and intraplate earthquakes. Although the current version of the inverse models assumes the trench axis type earthquake, northeast Japan is known to suffer from other types of tsunamis deriving from intra-plate earthquakes (e.g., 2022 Fukushima-oki tsunami), outer rise earthquake (e.g., 1933 Showa-Sanriku tsunami), or transoceanic tsunami occurred at another side of the Earth (e.g., 1960 Chilean earthquake tsunami). Incorporating various source fault models can contribute to disaster prevention planning in broader regions of the world.

## Notation

The symbols, units, and meanings are listed below.

Symbol	Units	Meaning
$a$	m	Reference height as defined by van Rijn (1993)
$a_2$	-	Correlation factor for sediment concentration
$C_{2D}$	$m^{1/2}/s$	2D Chezy coefficient
$C_a$	$kg/m^3$	Mass concentration at reference height
$C_{kmx}$	$kg/m^3$	Mass concentration at the bottom of the active layer
$d$	m	Depth below datum
$D$	m	Average slip displacement of the fault
$D_L$	m	Slip displacement of LS
$D_S$	m	Slip displacement of SLS
$D_s$	m	Representative diameter of sediment
$D^*$	-	Non dimensional particle diameter
$D_{50}$	m	Medium diameter of sediment
$F$	1/s	Coriolis parameter
$f_{BED}$	-	Factor for bed-load sediment transport
$f_{SUS}$	-	Factor for current-related suspended sediment transport
$G$	$m/s^2$	Acceleration due to gravity
$G_{\xi\xi}^{\xi\xi}$	$m^{1/2}$	Coefficients to transform curvilinear to rectangular coordinates
$G_{\eta\eta}$	$m^{1/2}$	Coefficients to transform curvilinear to rectangular coordinates
$h$	m	Water depth
$I_k^{fm}$	-	Ground-truth parameters used to produce the kth training data
$I_k^{NN}$	-	Predicted parameters by the DNN
$L$	km	Length of fault
$L_L$	km	Length of LS
$L_S$	km	Length of SLS
$m$	-	Sediment mobility number
$m_e$	-	Excess sediment mobility number
$Mo$	Nm	Seismic moment

$M_w$	Nm	Moment magnitude
$M_\xi$	m/s <sup>2</sup>	Source or sink of momentum in $\xi$ direction
$M_\eta$	m/s <sup>2</sup>	Source or sink of momentum in $\eta$ direction
$P$	kg/ms <sup>2</sup>	Water pressure
$s$	-	Relative density of sediment
$S$	km <sup>2</sup>	Area of fault
$S_L$	km <sup>2</sup>	Area of LS
$S_S$	km <sup>2</sup>	Area of SLS
$T_a$	-	Non dimensional bed shear stress
$u$	m/s	Flow velocities in $\xi$ direction
$v$	m/s	Flow velocities in $\eta$ direction
$v_{cr}$	m/s	Critical velocity for the initial motion of medium diameter of the diameter
$W$	km	Width of fault
$W_L$	km	Width of LS
$W_S$	km	Width of SLS
$w_s$	m/s	Particle settling velocity
$z_{kmx}$	m	Elevation of the center of the active layer
$\varepsilon_s$	m <sup>2</sup> /s	Sediment diffusion coefficient at the bottom of active layer
$\theta_c$	-	Shields parameter
$\nu$	m <sup>2</sup> /s	Kinematic viscosity coefficient of water
$\rho_0$	kg/m <sup>3</sup>	Density of water
$\rho_s$	kg/m <sup>3</sup>	Density of sediment
$\zeta$	m	Water level above datum

---

## **Acknowledgment**

I would like to express my gratitude to my supervisor, Dr. Hajime Naruse, Kyoto University, Division of Earth and Planetary Sciences, Department of Geology and Mineralogy, for his continuous support, patience, and encouragement for my research.

I would like to thank my collaborator, Dr. Daisuke Sugawara, Tohoku University, for his contribution to the preparation of the forward model.

I am thankful to the INPEX corporation for providing support during my Ph.D. program. Finally, I am grateful to my parents, my wife Mika Iijima, and my son Seiya Iijima, for their patience and support, encouragement and inspiration to complete my PhD program.

## Reference

- Abe, K., 1978. A dislocation model of the 1993 Sanriku earthquake consistent with the tsunami waves. *Journal of Physics of the Earth*, 26(4), 381-396.
- Abe, T., Goto, K., Sugawara, D., 2012. Relationship between the maximum extent of tsunami sand and the inundation limit of the 2011 Tohoku-oki tsunami on the Sendai plain, Japan. *Sedimentary Geology*, 282, 142-150.
- Abe, T., Goto, K., Sugawara, D., 2020. Spatial distribution and sources of tsunami deposits in a narrow valley setting – insight from 2011 Tohoku-oki tsunami deposits in northeastern Japan. *Progress in Earth and Planetary Science*, 7, 1-21.
- Apotsos, A., Gelfenbaum, G., Jaffe, B., Watt, S., Peck, B., Byckley, M., Stevens, A., 2011a. Tsunami inundation and sediment transport in a sediment-limited embayment on American Samoa. *Earth-Science Reviews*, 107, 1-11.
- Apotsos, A., Gelfenbaum, G., Jaffe, B., 2011b. Process-based modeling of tsunami inundation and sediment transport. *Journal of Geophysical research-Earth Surface*, 116, F01006.
- Arai, K., Naruse, H., Miura, R., Kawamura, K., Hino, R., Ito, Y., Inazu, D., Yokokawa, M., Izumi, N., Murayama, M., 2013. Tsunami-generated turbidity current of the 2011 Tohoku-Oki earthquake, *Geology*, 41, 1195-1198.
- Atwater, B. F., 1987. Evidence for Great Holocene Earthquakes Along the Outer Coast of Washington State. *Science*, 236, 942-944.
- Bondevik, S., Stormo, S. K., Skjerdal, G., 2012. Green mosses date the Storegga tsunami to the chilliest decades of the 8.2 ka cold event. *Quaternary Science Reviews*, 45, 1-6.
- Bourgeois, J., Hansen, T. A., Wiberg, P. L., Kauffman, E. G., 1988. A Tsunami Deposit at the Cretaceous-Tertiary Boundary in Texas. *Science*, 241, 567-570.
- Chagué-Goff, C., Andrew, A., Szczuciński, W., Goff, J., Nishimura, Y., 2012. Geochemical signatures up to the maximum inundation of the 2011 Tohoku-oki tsunami – Implications for the 869 AD Jogan and other paleo tsunamis. *Sedimentary Geology*, 282, 65-77.
- Cita, M. B., Camerlenghi, A., Rimoldi, B., 1996. Deep-sea tsunami deposits in the eastern Mediterranean: new evidence and depositional models. *Sedimentary Geology*, 104, 155-173.
- Costa, P. J., Andrade, C., Cascalho, J., Dawson, A. G., Freitas, M. C., Paris, R., and Dawson, S., 2015. Onshore tsunami sediment transport mechanisms inferred from heavy mineral assemblages. *The Holocene*, 25, 795-809.

- Costa, P. J., Andrade, C., 2020. Tsunami deposits: Present knowledge and future challenges. *Sedimentology*, 67, 1189-1206.
- Deltares, 2021. User Manual Delft3D-FLOW. 3.15.18392.
- Eshelby, J. D., 1957. The determination of the elastic field of an ellipsoidal inclusion, and related problems. *Proceedings of the Royal Society*, A241, 376-396.
- Fire and Disaster management Agency, 2020. Damage situation of the 2011 off the Pacific coast of Tohoku earthquake (Great East Japan Earthquake) on 2011 (As of 10 March 2020). (accessed 10<sup>th</sup> August 2023) (in Japanese).
- Fujino, S., Naruse, H., Matsumoto, D., Jarupongsakul, T., Sphawajruksakul, A., Sakakura, N., 2009. Stratigraphic evidence for pre-2004 tsunamis in southwestern Thailand. *Marine Geology*, 262, 25-28.
- Fujino, S., Naruse, H., Matsumoto, D., Sakakura, N., Suphawajruksakul, A., Jarupongsakul, T., 2010. Detailed measurements of thickness and grain size of a widespread onshore tsunami deposit in Phang-nga Province, southwestern Thailand. *Island Arc*, 19, 389-398.
- Fujiwara, O., Tanigawa, K., 2014. Bedforms record the flow conditions of the 2011 Tohoku-Oki tsunami on the Sendai Plain, northeast Japan. *Marine Geology*, 358, 79-88.
- Fujiwara, H., Hirata, K., Nakamura, H., Osada, M., Morikawa, N., Kawai, S., Ohsumi, T., Aoi, S., Matsuyama, H., Toyama, N., Kito, T., Murasima, Y., Murata, Y., Inoue, T., Saito, R., Akyama, S., Korenaga, M., Abe, Y., Hashimoto, N., 2015. An Approach to Tsunami Hazard Assessment along the Northeastern Coastal Area in Japan-Method and Preliminary Results-. Technical Note National Research Institute of Earth Science and Disaster Prevention, 400 (in Japanese)
- Geospatial Information Authority (GSI). Overview map of tsunami inundation area. <https://www.gsi.go.jp/kikaku/kikaku40014.html>. (Accessed 29th June 2021)
- Goff, J., Chague-Goff, C., Nichol, S., Jaffe, B., Dominey-Howes, D., 2012. Progress in paleotsunami research. *Sedimentary Geology*, 243-244, 70-88.
- Goto, C., Ogawa, Y., Shuto, N., Imamura, F., 1997. Numerical method of tsunami simulation with the leap-frog scheme. In: IUGG/IOC TIME project, IOC Manual and Guides, 35, pp. 1-126.
- Goto, K., Chavanich, S. A., Imamura, F., Kunthasap, P., Matsui, T., Minoura, K., Sugawara, D., Yanagisawa, H., 2007. Distribution, origin and transport process of boulders deposited by the 2004 Indian Ocean tsunami at Pakarang Cape, Thailand. *Sedimentary Geology*, 202, 821-837.

- Goto, K., Kawana, T., Imamura, F., 2010. Historical and geological evidences of boulders deposited by tsunamis, southern Ryuku Islands, Japan. *Earth-Science Reviews*, 102, 77-99.
- Goto, K., Chagué-Goff, C., Fujino, S., Goff, J., Jaffe, B., Nishimura, Y., Richmond, R., Sugawara, D., Szczuciński, W., Tappin, D.R., Witter, R.C., Yulianto, E., 2011. New insights of tsunami hazard from the 2011 Tohoku-oki event. *Marine Geology*, 290, 46-50.
- Goto, K., Chague-Goff, C., Goff, J., Jaffe, B., 2012. The future of tsunami research following the 2011 Tohoku-oki event. *Sedimentary Geology*, 282, 1-13.
- Goto, K., Hashimoto, K., Sugawara, D., Yanagisawa, H., Abe, T., 2014. Spatial thickness variability of the 2011 Tohoku-oki tsunami deposits along the coastline of Sendai Bay, *Marine Geology*, 358, 38-48.
- Goto, K., Ishizawa, T., Ebina, Y., Imamura, F., Sato, S., Udo, K., 2021. Ten years after the 2011 Tohoku-oki earthquake and tsunami: Geological and environmental effects and implications for disaster policy changes. *Earth-Science reviews*, 212, 103417.
- Gusman, A. R., Goto, T., Satake, K., Takahashi, T., Ishibe, T., 2018. Sediment transport modeling of multiple grain sizes for the 2011 Tohoku tsunami on a steep coastal valley of Numaonhama, northeast Japan. *Marine Geology*, 405, 77-91.
- Hatori, T., 2009. Regional deviation of inundation heights due to the large Sanriku tsunamis. *Rekishu Zishin (Historical Earthquake)*, 24, 41-48. (in Japanese with English abstract)
- Hayashi, S., Koshimura, S., 2013. The 2011 Tohoku tsunami flow velocity estimation by the aerial video analysis and numerical modeling. *Journal of Disaster Research*, 8(4), 561-572.
- Headquarters for Earthquake Research Promotion (HERP), 2017. Tsunami prediction method for earthquakes with characterized source faults (Tsunami Recipe). [https://www.jishin.go.jp/main/tsunami-e/17jan\\_tsunami-recipe.pdf](https://www.jishin.go.jp/main/tsunami-e/17jan_tsunami-recipe.pdf). (Accessed 15 November 2023)
- Hirano, M., 1971. River and degradation with armouring. *Japan Society of Civil Engineering Proceedings*, 195, 55-65. (in Japanese)
- Iijima, Y., Goto, K., Minoura, K., Komatsu, G., Imamura, F., 2014. Hydrodynamics of impact-induced tsunami over the Martian ocean. *Planetary and Space Sciences*, 95, 33-44.
- Iijima, Y., Goto, K., Sugawara, D., Abe, T., 2021. Effect of artificial structure on the formation process of the 2011 Tohoku-oki tsunami deposit. *Sedimentary Geology*, 423, 105978.

- Imamura, F., Koshimura, S., Mabuchi, Y., Oya, T., Okada, K., 2012. Tsunami simulation for the 2011 off the Pacific coast of Tohoku earthquake: Tohoku University model version 1.2. 12pp. (in Japanese)
- Ishimura, D., Yamada, K., 2019. Palaeo-tsunami inundation distances deduced from roundness of gravel particles in tsunami deposits. *Scientific reports*, 9, 1-8.
- Ishizawa, T., Goto, K., Yokoyama, Y., Miyairi, Y., Sawada, C., Nishimura, Y., Sugawara, D., 2017. Sequential radiocarbon measurement of bulk peat for high-precision dating of tsunami deposits. *Quaternary Geochronology*, 41, 202-210.
- Ishizawa, T., Goto, K., Yokoyama, Y., Miyairi, Y., 2019. Non-destructive analyses to determine appropriate stratigraphic level for dating of tsunami deposits. *Marine Geology*, 412, 19-26.
- Jaffe, B., Gelfenbaum, G., 2007. A simple model for calculating tsunami flow speed from tsunami deposits. *Sedimentary geology*, 200, 347-361.
- Jaffe, B., Goto, K., Sugawara, D., Gelfenbaum, G., La Selle, S., 2016. Uncertainty in tsunami sediment transport modeling. *Journal of Disaster Research*, 11, 647-661.
- Jagodziński, R., Sternal, B., Szczuciński, W., Chagué-Goff, C., Sugawara, D., 2012. Heavy minerals in the 2011 Tohoku-oki tsunami deposits – insights into sediment sources and hydrodynamics. *Sedimentary Geology*, 282, 57-64.
- Jankaew, K., Atwater, B. F., Sawai, Y., Choowong, M., Charoentitirat, T., Martin, M. E., Prendergast, A., 2008. Medieval forewarning of the 2004 Indian Ocean tsunami in Thailand. *Nature*, 455, 1228-1231.
- Japan Society of Civil Engineers, 2016. Tsunami Assessment Method for Nuclear Power Plants in Japan. 127pp. (in Japanese)
- Kon'no, E., 1961. Geological observations of the Sanriku coastal region damaged by tsunami due to the Chile earthquake in 1960. *Contributions to the Institute of Geology and Paleontology, Tohoku University*, 52, 1-40.
- Lay, T., 2018. A review of the rupture characteristics of the 2011 Tohoku-oki Mw 9.1 earthquake. *Tectonophysics*, 733, 4-36.
- Masaya, R., Suppasri, A., Yamashita, K., Imamura, F., Gouramanis, C., Leelawat, N., 2019. Investigating beach erosion related with its recovery at Phra Thong Island, Thailand caused by the 2004 Indian Ocean tsunami. *Natural Hazards and Earth System Sciences*, 20, 2823-2841.
- Matsui, T., Imamura, F., Takjika, E., Nakao, Y., Fujisawa, Y., 2002. Generation and propagation of a tsunami from the Cretaceous-Tertiary impact event. *Geological Society of America Special Paper*, 356, 69-77.

- Matsumoto, H., 1985. Beach Ridge Ranges and the Holocene Sea-Level Fluctuations on Alluvial Coastal Plains, northeast Japan. Scientific Report of Tohoku University, 7th series (Geography), 15-46.
- Matsumoto, D., Sawai, Y., Tanigawa, K., Fujiwara, O., Namegaya, Y., Shishikura, M., Kagohara, K., Kimura, H., 2016. Tsunami deposit associated with the 2011 Tohoku-oki tsunami in the Hasunuma site of the Kujukuri coastal plain, Japan. *Island Arc*, 25, 369-385.
- Melgar, D., Bock, Y., 2015. Kinematic earthquake source inversion and tsunami runup prediction with regional geophysical data. *Journal of Geophysical Research: Solid Earth*, 120, 3324-3349
- Minoura, K., Nakaya, S., Sato, H., 1987. Traces of Tsunamis Recorded in Lake Deposits - An Examples from Jusan, Shiura-mura, Aomori-. *Jisin*, 40, 183-196. (in Japanese with English abstract)
- Minoura, K., Nakaya, S., 1991. Traces of tsunami preserved in inter-tidal lacustrine and marsh deposits: some examples from northeast Japan, *The Journal of Geology*. 99, 265-287.
- Minoura, K., Nakaya, S., Uchida, M., 1994. Tsunami deposits in a lacustrine sequence of the Sanriku coast, northeast Japan. *Sedimentary Geology*, 89, 25-31.
- Minoura, K., Imamura, F., Sugawara, D., Kono, Y., Iwashita, T., 2001. The 869 Jogan tsunami deposit and recurrence interval of large-scale tsunami on the Pacific coast of northeast Japan. *Journal of Natural Disaster Science*, 23, 83-88.
- Mitra, R., Naruse, H., Abe, T., 2020. Estimation of Tsunami Characteristics from Deposits: Inverse Modeling using a Deep-Learning Neural network. *Journal of Geophysical Research: Earth Surface*, 125, e2020JF005583.
- Mitra, R., Naruse, H., Fujino, S., 2021. Reconstruction of flow conditions from 2004 Indian Ocean tsunami deposits at the Phra Thong island using a deep neural network inverse model. *Natural Hazards and Earth System Science*, 21, 1667-1683.
- Miyazawa, K., Goto, K., Imamura, F., 2012. Re-evaluation of the 1771 Meiwa Tsunami source model, southern Ryukyu Island, Japan. *Advances in Natural and Technological Hazards Research, Submarine Mass Movements and Their Consequences*, Springer, 31, 497-506.
- Moore, A., McAdoo, B. G., Ruffman, A., 2007. Landward fining from multiple sources in a sand sheet deposited by the 1929 Grand Banks tsunami, Newfoundland. *Sedimentary Geology*, 200, 336-346.

- Mori, N., Takahashi, T., the 2011 Tohoku earthquake tsunami joint survey group, 2012. Nationwide post event survey and analysis of the 2011 Tohoku earthquake tsunami. *Coastal Engineering Journal*, 54(1), 1-27.
- Morton, R. A., Gelfenbaum, G., Jaffe, B. E., 2007. Physical criteria for distinguishing sandy tsunami and storm deposits using modern examples. *Sedimentary Geology*, 200, 184-207.
- Nakamura, Y., Nishimura, Y., Putra, P.S., 2012. Local variation of inundation, sedimentary characteristics, and mineral assemblages of the 2011 Tohoku-oki tsunami on the Misawa coast, Aomori, Japan. *Sedimentary Geology*, 282, 216-227.
- Namegaya, Y., Satake, K., Yamamoto, S., 2010. Numerical simulation of the AD 869 Jogan tsunami in Ishinomaki and Sendai plains and Ukedo river-mouth lowland. *Annual Report of Active Fault Paleoseismic Research*, 10, 1-21. (in Japanese with English abstract)
- Namegaya, Y., Satake, K., 2014. Reexamination of the AD 869 Jogan earthquake size from tsunami deposit distribution, simulated flow depth, and velocity. *Geophysical Research Letters*, 41, 2297-2303.
- Naruse, H., Fujino, S., Suphawajruksakul, A., Jarupongsakul, T., 2010. Features and formation processes of multiple deposition layers from the 2004 Indian Ocean Tsunami at Ban Nam Kem, southern Thailand. *Island Arc*, 19, 399-411.
- Naruse, H., Arai, K., Matsumoto, D., Takahashi, H., Yamashita, S., Tanaka, G., Murayama, M., 2012. Sedimentary features observed in the tsunami deposits at Rikuzentakata City. *Sedimentary Geology*, 282, 199-215.
- Naruse, H., Abe, T., 2017. Inverse tsunami flow modeling including nonequilibrium sediment transport, with application to deposits from the 2011 Tohoku-oki tsunami. *Journal of Geophysical Research: Earth Surface*, 122, 2159-2182.
- Naruse, H., Nakao, K., 2021. Inverse modeling of turbidity currents using an artificial neural network approach: verification for field application. *Earth Surface Dynamics*, 9(5), 1091-1109.
- Nemoto, N., Minoura, K., 2012. Destruction of artificial beach ridge by shooting flow – an example of tsunami damage by the 2011 off the Pacific coast of Tohoku Earthquake along the eastern coast of Aomori Prefecture, Northeast Japan. *Earth Science (Chikyu Kagaku)*, 66, 209-210. (in Japanese)
- Nishimura, Y., Miyaji, N., 1995. Tsunami deposits from the 1993 Southwest Hokkaido earthquake and the 1640 Hokkaido Komagatake eruption, northern Japan. *Pure and applied geophysics*, 144, 719-733.

- Okada, Y., 1985. Surface deformation due to shear and tensile faults in a half-space. *Bulletin of the Seismological Society of America*, 75, 1135-1154.
- Omira, R., Ramalho, R. S., Kim, J., Gonzalez, P. J., Kardi, U., Miranda, J. M., Carriho, F., Baptista, M. A., 2022. Global Tonga tsunami explained by a fast-moving atmospheric source. *Nature*, 609, 734-740.
- Ozawa, S., Nishimura, T., Munekane, H., Suito, H., Kobayashi, T., Tobita, M., Imakiire, T., 2012. Preceding, coseismic, and postseismic slips of the 2011 Tohoku earthquake, Japan. *Journal of Geophysical Research*, 117, B07404.
- Pari, Y., Murthy, M. R., Kumar, J. S., Subramanian, B., Ramachandran, S., 2008. Morphological changes at Vellar estuary, India—Impact of the December 2004 tsunami. *Journal of Environmental management*, 89, 45-57.
- Paris, R., Lavigne, F., Wassemer, P. and Sartohadi, J., 2007. Coastal sedimentation associated with the December 26, 2004 tsunami in Lhok Nga, west Banda Ache (Sumatra, Indonesia). *Marine Geology*, 238, 93-106.
- Parker, G., 1991. Selective sorting and abrasion of river gravel. I: Theory. *Journal of Hydraulic Engineering*, 177(2), 131-147.
- Pham, D. T., Gouramanis, C., Switzer, A. D., Rubin, C. M., Jones, B. G., Jankaew, K., Carr, P. F., 2017. Elemental and mineralogical analysis of marine and coastal sediments from Phra Thong Island, Thailand: Insights into the provenance of coastal hazard deposits. *Marine Geology*, 385, 274-292.
- Phantuwongraj, S., Choowong, M., 2012. Tsunamis versus storm deposits from Thailand. *Natural Hazards*, 63, 31-50.
- Philibosian, B., Sieh, K., Avouac, J.-P., Natawidjaja, D. H., Chiang, H.-W., Wu, C.-C., Shen, C.-C., Daryono, M. R., Perfettini, H., Suwargadi, B. W., 2017. Earthquake supercycles on the Mentawai segment of the Sunda megathrust in the seventeenth century and earlier. *Journal of Geophysical Research: Solid Earth*, 122, 642-676.
- Quenouille, M., 1949. Approximate tests of correlation in time-series. *Journal of the Royal Statistical Society B*, 11, 68-84.
- Richmond, B., Szczuciński, W., Chagué-Goff, C., Goto, K., Sugawara, D., Witter, R., Tappin, D.R., Jaffe, B., Fujino, S., Nishimura, Y., Goff, J., 2012. Erosion, deposition and landscape change on the Sendai coastal plain, Japan, resulting from the March 11, 2011 Tohoku-oki tsunami. *Sedimentary Geology*, 282, 27-39.
- Robke, B. R., Vott, A., 2017. The tsunami phenomenon. *Progress in Oceanography*, 159, 296-322.

- Rubin, C. M., Horton, B. P., Sieh, K., Pilarczyk, J. E., Daly, P., Ismail, N., Parnell, A. C., 2017. Highly variable recurrence of tsunamis in the 7,400 years before the 2004 Indian Ocean tsunami. *Nature communications*, 8, 1-12.
- Sanuki, H., Takemori, R., Tajima, Y., Sato, S., 2013. Study on tsunami flooding in river based on video images and numerical simulation. *Proceedings of Coastal Engineering, JSCE*, 69, 196-200.
- Satake, K., Namegaya, Y., Yamamoto, S., 2008. Numerical simulation of the AD 869 Jogan tsunami in Ishinomaki and Sendai plains. *Annual Report of Active Fault Paleoseismicity Research*, 8, 71-89. (in Japanese with English abstract)
- Satake, K., Fujii, Y., Harada, T., Namegaya, Y., 2013. Time and space distribution of coseismic slip of the 2011 Tohoku earthquake as inferred from tsunami waveform data. *Bulletin of Seismology Society of America*, 103, 1473-1492.
- Sato, H., Shimamoto, T., Tsutsumi, A., Kawamoto, E., 1995. Onshore tsunami deposits caused by the 1993 southwest Hokkaido and 1983 Japan-sea earthquakes. *Pure and applied geophysics*, 144, 693-717.
- Sawai, Y., Jankaew, K., Martin, M. E., Prendergast, A., Choowong, M., Charoentitirat, T., 2009. Diatom assemblages in tsunami deposits associated with the 2004 Indian Ocean tsunami at Phra Thong Island, Thailand. *Marine Micropaleontology*, 73, 70-79.
- Sawai, Y., Namegaya, Y., Okamura, Y., Satake, K., Shishikura, M., 2012. Challenges of anticipating the 2011 Tohoku earthquake and tsunami using coastal geology. *Geophysical Research Letters*, 39, I\_L21309.
- Seno, T., 2012. Great earthquake along the Nankai Trough - a new idea for their rupture mode and time series-. *Zisin*, 64, 97-116. (in Japanese with English abstract)
- Shiki, T., Yamazaki, T., 2008. The term “tsunamiite”, in: *Tsunamiites*, pp. 5-7, Elsevier.
- Shinozaki, T., Fujino, S., Ikehara, K., Sawai, Y., Tamura, T., Goto, K., Sugawara, D., Abe, T., 2015. Marine biomarkers deposited on coastal land by the 2011 Tohoku-oki tsunami. *Natural Hazards*, 77, 445-460.
- Soulsby, R., Smith, D., Ruffman, A., 2007. Reconstructing tsunami run-up from sedimentary characteristics – a simple mathematical model. *Coastal Sediment*, 7(2), 1075-1088.
- Sugawara, D., Imamura, F., Matsumoto, H., Goto, K., Minoura, K., 2010. Quantitative reconstruction of a paleo-tsunami: field survey of Jogan tsunami and paleotopography. *DCRC Tsunami Engineering*, 27, 103-132.
- Sugawara, D., Imamura, F., Matsumoto, H., Goto, K., Minoura, K., 2011. Reconstruction of the AD 869 Jogan earthquake induced tsunami by using the

- geological data. *Journal of Natural Disaster Science*, 20, 501-516. (in Japanese with English abstract)
- Sugawara, D., Goto, K., 2012. Numerical modeling of the 2011 Tohoku-oki tsunami in the offshore and onshore of Sendai Plain, Japan. *Sedimentary Geology*, 282, 110-123.
- Sugawara, D., Imamura, F., Goto, K., Matsumoto, H., Minoura, K., 2013. The 2011 Tohoku-oki earthquake tsunami: similarities and differences to the 869 Jogan tsunami on the Sendai plain. *Pure and applied geophysics*, 170, 831-843.
- Sugawara, D., Takahashi, T., Imamura, F., 2014. Sediment transport due to the 2011 Tohoku-oki tsunami at Sendai: result from numerical modeling. *Marine Geology*, 358, 18-37.
- Szczuciński, W., Kokociński, M., Rzeszewski, M., Chagué-Goff, C., Cachão, M., Goto, K., Sugawara, D., 2012. Sediment sources and sedimentation processes of 2011 Tohoku-oki tsunami deposits on the Sendai Plain, Japan – Insights from diatoms, nanoliths and grain size distribution. *Sedimentary Geology*, 282, 40-56.
- Takashimizu, Y., Urabe, A., Suzuki, K., Sato, Y., 2012. Deposition by the 2011 Tohoku-oki tsunami on coastal lowland controlled by beach ridges near Sendai, Japan. *Sedimentary Geology*, 282, 124-141.
- Van Rijn, L. C., 1993. *Principles of Sediment Transport in Rivers, Estuaries and Coastal Seas*. Aqua Publication, The Netherlands, 654 pp.
- Watanabe, M., Goto, K., Bricker, J. D., Imamura, F., 2018. Are inundation limit and maximum extent of sand useful for differentiating tsunamis and storms? An example from sediment transport simulations on the Sendai Plain, Japan. *Sedimentary Geology*, 364, 204-216.
- Yamashita, K., Sugawara, D., Takahashi, T., Imamura, F., Saito, Y., Imato, Y., Kai, T., Uehara, H., Kato, T., Nakata, K., Saka, R., Nishikawa, A., 2016. Numerical simulations of large-scale sediment transport caused by the 2011 Tohoku Earthquake Tsunami in Hirota bay, Southern Sanriku Coast. *Coastal Engineering Journal*, 58(4), 1640015.